CHINESE OPTICS LETTERS

Vol. 19, No. 9 | September 2021

Mode division multiplexing: from photonic integration to optical fiber transmission [Invited]

Jiangbing Du (杜江兵)*, Weihong Shen (沈微宏), Jiacheng Liu (刘嘉程), Yufeng Chen (陈宇峰), Xinyi Chen (陈心怡), and Zuyuan He (何祖源)**

State Key Laboratory of Advanced Optical Communication Systems and Networks, Shanghai Jiao Tong University, Shanghai 200240, China

*Corresponding author: dujiangbing@sjtu.edu.cn

**Corresponding author: zuyuanhe@sjtu.edu.cn

Received December 29, 2020 | Accepted February 26, 2021 | Posted Online August 23, 2021

To overcome the capacity crunch of optical communications based on the traditional single-mode fiber (SMF), different modes in a few-mode fiber (FMF) can be employed for mode division multiplexing (MDM). MDM can also be extended to photonic integration for obtaining improved density and efficiency, as well as interconnection capacity. Therefore, MDM becomes the most promising method for maintaining the trend of "Moore's law" in photonic integration and optical fiber transmission. In this tutorial, we provide a review of MDM works and cutting-edge progresses from photonic integration to optical fiber transmission, including our recent works of MDM low-noise amplification, FMF fiber design, MDM Si photonic devices, and so on. Research and application challenges of MDM for optical communications regarding long-haul transmission and short reach interconnection are discussed as well. The content is expected to be of important value for both academic researchers and industrial engineers during the development of next-generation optical communication systems, from photonic chips to fiber links.

Keywords: mode division multiplexing; photonic integration; few-mode fiber; optical transmission; optical interconnection.
DOI: 10.3788/COL202119.091301

1. Introduction

In a multimode optical waveguide, the light wave propagates in different paths, exhibiting different field distributions, so-called orthogonal modes. Optical field density can be significantly strengthened when multiple orthogonal modes are co-propagating in the same waveguide while maintaining acceptable or even improved performance of attenuation, dispersion, nonlinearity, signal quality, and so on. Such kinds of co-propagation of multiple orthogonal modes in one waveguide are called mode division multiplexing (MDM), which was first, to the best of our knowledge, brought up tens of years ago (as early as 1982[1]) and now is revived again due to the "Moore's law" demand of optical communication capacity and photonic integration. "Moore's law" in optical communication is even more serious than its original interpretation in microelectronics, no matter whether it is for photonic integration density or optical fiber transmission capacity.

1.1. "Moore's law" for photonic integration

Photonic integration is a kind of microelectronic technology. However, it does not obey "Moore's law" of conventional microelectronics, which has exponential development in the number of transistors per chip (100% increase per ~18 months). The basic reason is that the lightwave is at the micron-scale, which is much larger than electrons as well as electrical transistors. Meanwhile, the transmission and gating behavior of lightwaves are intrinsically different compared with electrons. Even so, quasi-"Moore's law" development of photonic integration can still be observed due to the rapid development of photonic integration technologies (at their earlier stages), including silicon (Si) photonics (SIP), planar lightwave circuits (PLCs), III-V material integration, and so on.

From the historical view of microelectronics development, as presented in Fig. 1 (lower), "Moore's law" has been well maintained (and is yet not dead) for continuously increasing the application specific integrated circuit (ASIC) integration density. Space division multiplexing (SDM) methods are also included in ASIC integration, which is well known as 2.5/three-dimensional (3D) stacking for packaging. The fabrication process is still developing and is now approaching 3 nm. Below 3 nm, the processes are getting more and more difficult. Therefore, SDM based on 2.5/3D stacking could play a very important role in maintaining "Moore's law".

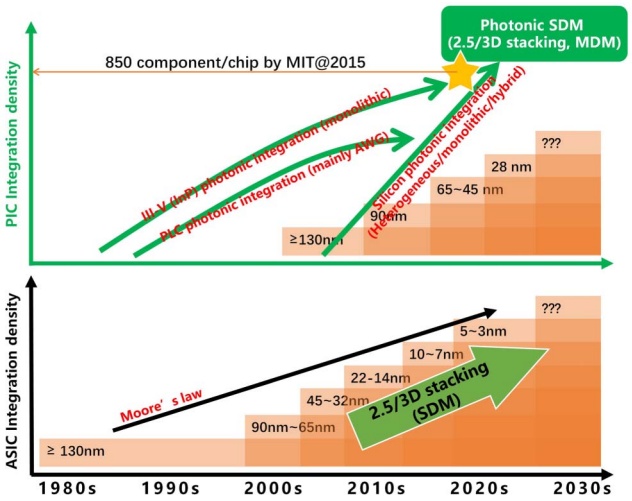

Fig. 1. Historical view of microelectronics development, PIC integration (upper), and ASIC integration (lower).

On the other hand, after more than three decades of development, photonic integrated circuit (PIC) integration is now stepping into the 28 nm process. However, most PIC integration platforms are still using the old fashioned process like 130 nm, 90 nm, and 45 nm, with balanced consideration of performance and cost. A very interesting situation is that improvement of process cannot lead to the steady improvement of integration density of PICs, which is limited by the intrinsic property of lightwaves. Then, inevitably, there will be a ceiling for PIC integration density, no matter how the advanced processes are utilized. Therefore, it is very difficult to realize large-scale photonic integration, and currently the largest amount of photonic components per chip is only about 850 by Massachusetts Institute of Technology (MIT)[2], which is a million times smaller than the transistor amount in ASIC. However, it does not mean the death of "Moore's law" for photonic integration.

As shown in Fig. 1 (upper), the development of PICs (PLC, III-V, and SIP) will eventually step into SDM, just like ASICs. The difference is that photonic SDM is not just about 2.5/3D stacking. MDM can also be utilized here due to the intrinsic Boson property of lightwaves. The "Moore's law" trend for photonic integration can thus be well maintained.

There are two different benefits for MDM in photonic integration: improved signaling density with more data in the same waveguide and improved efficiency with reduced power consumption for active devices. All of them are aimed at integration density. Together with 2.5/3D stacking and MDM, one can expect very a promising future for photonic integration. In this paper, we will talk about MDM out of photonic SDM.

1.2. "Moore's law" for optical fiber transmission

As for optical fiber communication, more typically optical fiber transmission, the capacity crunch of the conventional single-mode fiber (SMF) is almost approached, based on the encouraging development of optical communication technologies in

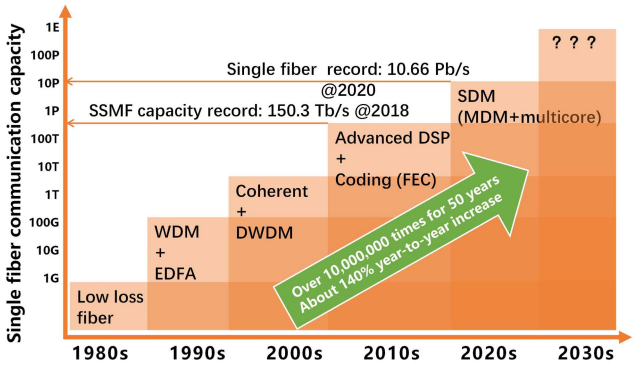

Fig. 2. Optical fiber transmission capacity trend with respect to all kinds of enabling technologies.

the past five decades[3]. The enabling technologies include mainly low-loss fibers in the 1980s, erbium-doped fiber amplifiers (EDFAs) in the 1990s, wavelength division multiplexing (WDM) around 2000 (decades before and after 2000), advanced modulation with enhanced digital signal processing (DSP) in the 2010s, as well as advanced coding methods like forward error correction (FEC) since the 2010s[4].

Thus, 2020 is a special year, marking the end of a decade as well as the end for increasing trends of optical fiber transmission capacity based on the above-mentioned conventional technologies. The 50th anniversary of optical fibers also occurred in 2020, which brings up the new challenge of optical fiber transmission: what can we do to maintain the trend for the upcoming demand?

Presented in Fig. 2 are the historical trends of optical fiber transmission: the single-fiber capacity increases due to all kinds of technologies. Similar summarizations can also be found in Ref. [5] by D. J. Richardson *et al.* and Ref. [6] by T. Mizuno *et al.* The agreement for all of them is that SDM, including most importantly MDM, is the next answer for maintaining this "Moore's law" trend of optical fiber transmission capacity.

The current capacity record for standard SMFs (SSMFs) is 150.3 Tb/s[7], which is built up by dense WDM (DWDM) over S/C/L widebands, coherent modulation, and detection with polarization division multiplexed (PDM) 128 quadrature amplitude modulation (QAM). Enabled by MDM and multi-core fiber SDM, the single-fiber capacity record was boosted to 10.66 Pb/s in 2020[8].

Obviously, multi-core and MDM can be utilized simultaneously in SDM, but only MDM offers the intrinsic efficiency multiplexing of more data within the constraint space. Meanwhile, MDM is based on the few-mode fiber (FMF), which is more compatible with the SSMF system in terms of fabrication simplicity, cabling, maintenance, device, and so on. Therefore, we only focus on MDM out of SDM in this paper.

1.3. This paper

To make it clear, the key property of MDM is intrinsically the strengthened optical density in terms of signal transmission capacity, modulation efficiency, nonlinear efficiency, circuit size,

and so on. Thus, MDM provides us with advantages for very broad and colorful applications, not only for optical communications, but also for imaging, endoscopy, spectroscopy, power combination, lasing, sensing, optical computing, and so on. In this review paper, we will talk about the perspective of optical communication, including, particularly, optical fiber transmission and photonic integration.

Versatile routes of MDM can be applied to different applications. As for photonic integration, TE/TM/transverse electromagnetic (TEM) MDM is currently the only solution due to the special waveguide structure. As for optical fiber transmission, linear polarization (LP) and orbital angular momentum (OAM) can both be utilized. LP MDM well utilizes the space of the optical fiber. It has good compatibility of fabrication, splicing with conventional SMFs. Meanwhile, its performances of attenuation, bending, nonlinear coefficient, dispersion, and so on are comparable with conventional SMFs. Generally speaking, LP MDM is a more natural upgrade solution with respect to the current SMF solution. OAM MDM is also an attractive solution with high scalability, which can be expected to be highly useful for the ultra-large capacity links. As for LP MDM, there is strongly coupled MDM and weakly coupled MDM. Currently, weakly coupled MDM is rather attractive for short reach applications, in which multiple-input multiple-output (MIMO)-less MDM for reduced cost and stable transmission for robust field applications is highly demanded. However, for long-haul optical transmission, strongly coupled MDM would be attractive, since reduced nonlinearity and reduced MIMO complexity can be expected.

This review paper consists of four sections. The background and motivation of MDM are introduced in Section 1. MDM photonic integration, including platforms, interface devices, passive devices, active devices, and so on, is presented in Section 2. In Section 3, MDM fibers, devices, and systems for large capacity optical fiber transmission are discussed. Section 4 is the conclusion, where the challenges and future trends of MDM for optical communications are discussed as well.

2. MDM Photonic Integration

2.1. Platforms for MDM photonic integration

This section will briefly introduce five material platforms for MDM photonic integration, including Si, Si nitride (SiN), chalcogenides, lithium niobite (LN), and indium phosphide (InP), and discuss the optical characteristics, fabrication process, and the recent works on MDM.

2.1.1. Silicon

Si is a mature photonic integration platform that has been widely used to pattern various passive and active devices for decades. The typical Si waveguide uses Si as the core material and Si dioxide (SiO_2) or air as the cladding. The refractive index of Si (~3.4) is pretty high compared with air or the SiO_2 cladding layer, and hence strong optical guiding is guaranteed in the waveguide at the near-infrared wavelength. Besides, the strong optical confinement of Si allows for optical devices with a compact footprint. The Si-on-insulator (SOI) platform possesses plenty of advantages, including wide availability, low cost, and compatibility with mature complementary metal–oxide–semiconductor (CMOS) technology, which makes it one of the most prominent platforms for PICs.

The Si platform is suitable for MDM integration, as the propagation constant of the different spatial modes can be engineered to differ significantly thanks to the high core-cladding (Si/SiO_2) index contrast. For the Si waveguide with a fixed thickness, one could continuously tune the propagation constant of the different spatial modes by varying the waveguide width. When the propagation constants of two closely placed waveguides match each other, the spatial mode will convert from one waveguide to the other. Various Si-based on-chip mode (de)multiplexers (MUXs) for MDM have been demonstrated in past years. Some typical structures of mode (de)MUX for MDM include multimode interferometers, asymmetric Y junctions, adiabatic couplers, and asymmetric directional couplers (ADCs)[9–14], which we will discuss later in detail.

During the past decades, mode (de)MUXs for MDM on SOIs have been heading towards higher capacity and broader bandwidth. By introducing dual polarization to the mode (de)MUX, the number of mode channels can be increased up to 10[15]. The mode (de)MUXs are also be considered to work through a broad wavelength band in order to integrate with WDM devices[16]. A 64-channel hybrid (de)MUX was also developed to enable MDM and WDM simultaneously by integrating a four-channel broadband ADC mode (de)MUX and 16-channel arrayed-waveguide gratings[17].

2.1.2. Silicon nitride

SiN provides an alternative moderate-index-contrast system that is manufacturable in the CMOS environment[18]. The SiN membrane is typically deposited by either low pressure chemical vapor deposition (LPCVD) at high temperature ($>$ 700°C) or by plasma enhanced chemical vapor deposition (PECVD) at low temperature ($<$400°C). LPCVD-based SiN often has a refractive index of around 2.0 at the wavelength of 1550 nm. PECVD-based nitride can be Si-rich (higher refractive index) or nitrogen-rich (lower refractive index).

For the SiN waveguide, Si_3N_4 is employed as the core layer and SiO_2 as the cladding material. The difference of refractive index values between core and cladding allows a compact structure of the optical waveguide. SiN has some unique advantages compared to Si. First of all, SiN has a transparency window over the range from 400 to 2350 nm, which is broader than Si (1100 to 3700 nm) and is very suitable for applications requiring shorter wavelengths (e.g., data communication at 850 nm). Besides, SOI-based photonic wires have typical waveguide losses of 1 to 2 dB/cm, mainly because of the low scattering loss originating from the sidewall roughness. For SiN waveguides, the propagation loss can be reduced down to an order of magnitude, typically in the range of 0.3–1.0 dB/cm. For nonlinear applications,

SiN has the weaker Kerr nonlinearity than Si but the two-photon absorption (TPA) is virtually zero thanks to the material's large bandgap. Therefore, it has been proved to be well suited for on-chip nonlinear progress, such as frequency comb generation or supercontinuum generation.

Compared with Si, fewer MDM works have been done on the SiN platform. In Ref. [19], a three-mode MDM-WDM circuit on a SiN-on-silica substrate using ADCs and a micro-ring resonator (MRR) was demonstrated and shown to be able to support a 30 Gb/s data transmission for each channel separately.

2.1.3. Chalcogenide

Chalcogenide glass (ChG) contains a major constituent of the chalcogen elements from group 6a of the periodic table (sulphur, selenium, and tellurium, but excluding oxygen), covalently bonded to network formers such as As, Ge, Sb, Ga, Si, or P. Employing a high refractive index of $n \approx 2$–3, ChG films for waveguide fabrication could be produced by thermal evaporation[20], sputtering[21], chemical vapor deposition[22], and pulsed laser deposition[23]. The propagation loss of the chalcogenide waveguide drastically depends on its size. A small strip waveguide with mode areas around $0.2\,\mu m^2$ has loss around 1.5 dB/cm. For larger waveguides, the optical loss can be further reduced to 0.05 dB/cm at 1550 nm[24].

ChGs show promising application in various areas such as phase-change memories, solar cells, sensors, frequency conversion, and supercontinuum generation. The material nonlinearity of chalcogenides combined with the strong confinement and dispersion engineering achievable in the chalcogenide waveguide makes them attractive to form ultra-fast nonlinear devices. There are no free-carriers or TPA effects in chalcogenide materials. Meanwhile, these ChGs also have good mid-infrared transparency, thus supporting the applications like mid-infrared spectroscopy, which attracts growing interests because of its coverage over the characteristic spectral absorption features for many molecules. On-chip MDM interconnection at the 2 μm waveband was demonstrated on the ChG-on-dioxide platform, holding 3×80 Gb/s high-speed transmission[25].

2.1.4. Lithium niobate

The LN photonics platform has been an attractive platform over the past decades, due to its excellent material properties including the wide optical transparency window and high refractive index. Conventional LN waveguides are fabricated by titanium indiffusion or proton exchange, which typically form a low refractive index contrast[26]. The resulting large optical mode size and difficult growing on a SiO_2 substrate are the main reasons why it was not widely used as a functional part integrated on an SOI platform. When the process of single-crystal, sub-micrometer-thick LN film bonded on the top of a low-index substrate (SiO_2) was demonstrated and became commercially available[27], more researchers began to focus on this functional material. By using this thin film $LiNbO_3$ (TFLN) wafer, waveguides were created with high index contrast of > 0.7 and tightly optical modes.

However, etching of $LiNbO_3$ is a difficult task. Crystalline LN cannot be easily patterned due to its high chemical stability. As for traditional optical lithography, different hard masks such as hydrogen silsesquioxane (HSQ)[27] and chromium (Cr)[28] have been used for dry etching the LN layer. Optical lithography often leaves behind a surface roughness of a few nanometers on the sidewall, resulting in the propagation loss of the etched waveguide in the range of 0.4 dB/cm to 3 dB/cm. Recently a novel pathway of LN layer etching was demonstrated using chemo-mechanical polish lithography (CMPL)[29]. Thanks to the smooth surface polished by CMPL (surface roughness 0.452 nm), the propagation loss of the LN waveguide can be reduced to 0.027 dB/cm. Notably, the LN waveguide etched by this process is often larger than that patterned by dry etching, which is mainly limited to the precision of the CMPL process.

LN has several excellent material properties including the large electro-optic (EO) modulation properties originating from the Pockels effect, the high second-order nonlinear susceptibility, and piezoelectric response, so that it was widely used to demonstrate various functionalities such as ultra-fast EO modulation, EO frequency comb, and second harmonic generation. As for the MDM application, Jin and co-workers demonstrated a mode switch based on the proton-exchanged LN waveguide, which can switch between the fundamental mode and higher-order mode with an extinction ratio of ~18 dB[30].

2.1.5. Indium phosphide

The most attractive characteristic of InP is its possibility to integrate passive and active devices (lasers, light amplifiers, modulators, and detectors) in a single membrane. A typical InP waveguide is formed on the InP-membrane-on-Si (IMOS). The thickness of the membrane is chosen in the range of 250–300 nm. InP has a high refractive index of 3.17, leading to compact photonic devices. The single-mode waveguide with the cross section of 250 nm × 450 nm was commonly chosen.

The InP membrane can be bonded on a Si wafer through benzocyclobutene (BCB) adhesive polymer[31]. A thin layer of SiO_2 is coated to promote adhesion between the Si wafer and InP membrane. After bonding and baking, the InP substrate can be removed by wet etching. Notably, the thickness of the polymer layer can be conveniently tuned over a large range (from 50 nm up to 20 μm), which enables high flexibility of the platform scheme. The InP membrane can then be patterned to different functional devices through electron beam lithography and dry etching. However, in order to obtain a low-loss InP waveguide, the ratio between physical and chemical etching should be carefully determined to reduce the sidewall roughness. To date, a record-low value of 2.5 dB/cm loss for the InP waveguide is achieved[32].

Due to the long-term development of InP material and devices, many passive devices used for MDM like a mode MUX and polarization converter have been demonstrated. For instance, a novel type of waveguide polarization converter that converts the

Table 1. Photonic Integration Platforms.

	SOI	SiN	ChG	LN	InP
Index	3.4	2.0	2–3	2.6	3.2
Loss (dB/cm)	0.1	<0.01	0.05	0.027	0.3
Window (μm)	1.1–3.7	0.4–2.4	1.5–12	0.4–5	1.3, 1.5
Lasing	No	No	No	No	Yes
PD	Yes	No	No	No	Yes
Modulation	Yes	No	No	Yes	Yes
	Extra doping	/	/	Standard process	Standard process
CMOS compatibility	Yes	Yes	No	No	No

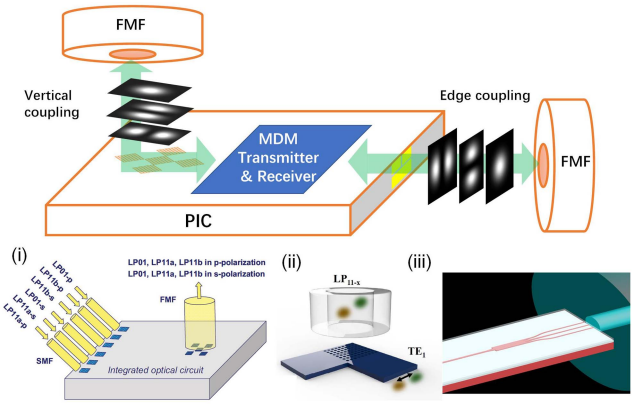

Fig. 3. Schematic diagram of MDM optical interface, including vertical coupling with on-chip mode multiplexer (MUX) and edge coupling with 3D asymmetric waveguide. (i)–(iii) Specific progresses of the MDM interface[35,36,37].

TE_0 mode to the TM_0 mode with efficient mode conversion of 0.4 dB loss and 16.6 dB extinction ratio was demonstrated numerically[33]. A mode MUX based on a multimode interferometer coupler used for converting the fundamental TE mode to a higher-order mode was demonstrated with a mode extinction ratio below 24 dB and low insertion loss below 0.7 dB[34].

A comprehensive comparison has been made in Table 1 regarding these fiber photonic integration platforms.

2.2. MDM interface for PIC-fiber coupling

Interface coupling builds an indispensable bridge that connects the optical signal from integrated waveguides to fiber transmission. The chip-to-fiber coupler can typically be classified into two types, vertical grating coupler (GC) and edge coupler, which have their own merits and have already been well investigated in the last decades. However, when it comes to multimode coupling, it becomes more complicated to maintain all of the guided modes having high coupling efficiency. In this section, we review the recent works on multimode interfaces for coupling between multimode waveguides on PICs and FMFs, as depicted in Fig. 3. Their practical application for an MDM transponder is also discussed. The summary of some typical MDM interfaces on SOI is listed in Table 2.

2.2.1. Grating coupler

As for the GC for higher-order mode coupling in FMFs, a straightforward method is to multiply the number of GCs so that each GC can correspondingly emit each lobe in the high-order mode (HOM). For instance, a double-part GC was employed to convert the TE_1 mode in the waveguide into the LP_{11} mode in the FMF, with a peak coupling efficiency of −3.68 dB[38]. An apodized GC composed of two sides with half-of-period offset, which creates a π phase difference between each other, was designed to realize TE_0-to-LP_{11} mode conversion with coupling loss of 3.1 dB[39]. Similarly, non-uniform gratings along the propagation direction can also generate π phase difference so as to form an LP_{11}/LP_{21} output field[40]. However, the above structures are specially designed for one specific HOM and unable to be used for fundamental mode LP_{01} and several HOMs simultaneously in the same design.

Table 2. Cutting-Edge Performance of MDM Interface on SOI.

	Vertical Coupling		Edge Coupling
Properties	**Ref. [35]**	**Ref. [36]**	**Ref. [37]**
Mode number	6	4	2
Coupling loss	20–25 dB	4.9–6.1 dB	10.77 dB
Crosstalk	/	−6 dB	−7.3 to −11.9 dB
Bandwidth	~30 nm	20 nm	>100 nm
Footprint/length	mm-scale	622 μm × 622 μm	<300 μm

In order to support multimode coupling, Koonen *et al.* proposed a Si PIC mode MUX with five parts of two-dimensional (2D) GC, which can support six polarization modes ($LP_{01,x}$, $LP_{01,y}$, $LP_{11,a,x}$, $LP_{11,a,y}$, $LP_{11,b,x}$, $LP_{11,b,y}$) excited from the PIC to FMF[35], as shown in Fig. 3, panel (i). This structure is also practicable for $LP_{21,a}$ and LP_{02} modes and presents low crosstalk among HOMs. Besides, the circuit was packaged with the FMF, 6-SMF array, and electrical control system and applied in a 3.072 Tb/s MDM and WDM transmission system as the mode MUX and deMUX[41]. A similar design with four parts of 2D GC was demonstrated in Refs. [42,43]. Theoretically, with more spots of GC settled in a specially arranged shape, this scheme has the scalability to support more HOMs in the FMF[44]. However, the large coupling loss (> 20 dB in Ref. [41]) and complicated phase control system may get worse as the mode number increases.

Another scheme is using a single GC to selectively launch several modes with high efficiency. Tong *et al.* demonstrated a novel multimode GC by genetic optimization, supporting four LP modes ($LP_{01,x}$, $LP_{01,y}$, $LP_{11,x}$, $LP_{11,y}$) with low coupling loss of 4.9 dB for LP_{01} and 6.1 dB for LP_{11}[36], as shown in Fig. 3, panel (ii). Although the mode crosstalk is not suppressed well (−6 dB), the proposed MUX was successfully employed in 4×40 Gb/s MDM transmission over the 15 m FMF. Thus, the structure with a single GC is more competitive as the multimode interface with the FMF in the MDM transponder thanks to its lower coupling loss, despite having less mode scalability compared to the scheme with several grating parts.

2.2.2. Edge coupler

Generally, the edge coupler is based on the inverse taper waveguide leaking the optical field into the cladding layer with a larger field diameter so as to decrease the mode mismatch between integrated waveguide and Si fiber. As for HOMs, e.g., LP_{11}, we can adopt the edge coupler with two individual inverse tapers to match the two lobes of the LP_{11} mode field[45], similar to the two-part GC for LP_{11} vertical coupling as we mentioned before. Besides, via a triple-tip inverse taper, LP_{01} and LP_{11} can simultaneously be excited and coupled[46,37], as shown in Fig. 3, panel (iii). However, such a structure can hardly be applied to vertical HOM.

In Ref. [47], a multi-stage SOI inverse taper buried in SiN cladding was designed to excite six polarization modes in the FMF, whereas the mode hybridization needs a pretty large length of 2.3 mm in total, which is impractical. Different from the highly compact Si PIC, a polymer material has a similar refractive index with the Si fiber, so that it is quite easy for polymer waveguides to transfer the guided modes into the FMF and also to fabricate a multi-layer structure to support vertical HOMs. In Ref. [48], a polymer multimode edge coupler based on 3D asymmetric waveguide branches was proposed for four modes (LP_{01}, $LP_{11,a}$, $LP_{11,b}$, $LP_{21,a}$) with a small coupling loss of <0.6 dB for all four modes despite the large mode converter (MC) loss in the polymer device. Thus, a polymer may be more suitable for multimode edge coupling between integrated waveguides and the FMF, but not better than Si devices for MCs.

2.3. Passive devices

Passive devices constitute a significant foundation in MDM photonic integrated systems for the mode multiplexing/demultiplexing and the propagation and routing of multimode signals. This section will introduce recent researches on multimode waveguiding devices, power coupling devices, and mode and wavelength manipulating devices, mainly focusing on the SOI platform. Multimode passive devices with small size, low loss, low modal crosstalk, and high scalability are mainly discussed.

2.3.1. Waveguide devices: bend and crossing

Generally, in a standard Si layer with 220 nm thickness, a 500-nm-wide single-mode waveguide can be bent by a 10 μm radius with negligible bending loss. While for a multimode waveguide, it is far more sensitive to the bend due to the much wider mode field. There will be extra scattering loss since the leakage into the cladding at the bending area will be severely affected by the sidewall roughness. Therefore, a multimode bent waveguide with a smaller bending radius under acceptable low bending loss is quite important for a dense MDM integrated system. Here, we introduce three kinds of multimode waveguide bends for MDM photonic integration. The benchmark performances of different MDM bends are summarized in Table 3.

The first one is based on the optimized curve, for instance, the Euler bend with a 45 μm effective radius for four TM modes and <0.5 dB bending loss[49], as shown in Fig. 4(a). The Bezier bend can support three TE modes at 20 μm effective radius and maintain <0.2 dB loss[52]. The MDM bends with an optimized curve present low bending loss, while the lower degree of optimizable parameters makes it hard to compact the bending radius down to an ultra-small size.

The second one is to introduce an MC before and after the bent waveguide in order to match the mode field in the straight waveguide and bent waveguide, like the subwavelength grating-based MC in Ref. [53]. Besides, a compact bent waveguide with 10 μm radius including MC length was applied for two TE modes with <0.2 dB loss and <−23 dB crosstalk[54]. These two kinds of structures easily obtain a multimode bend at tens of microns radius with low insertion loss, low crosstalk, and wide bandwidth. Similarly, moving the MC into the bending region,

Table 3. Benchmark Performance of MDM Bend.

Properties	Euler Bend[49]	SWG Bend[50]	Pixelated Bend[51]
Structure and principle	Waveguide curve optimization	SWG for mode converting	Inverse design of pixelated structure
Mode number	4 TM modes	6 modes with dual polarizations	4 TE modes
Bending radius	45 μm	10 μm	3.9 μm
Loss	<0.5 dB	<0.23 dB	<1.8 dB
Crosstalk	<−20 dB	<−26.5 dB	<−17 dB
Scalability	Yes	Yes	Yes

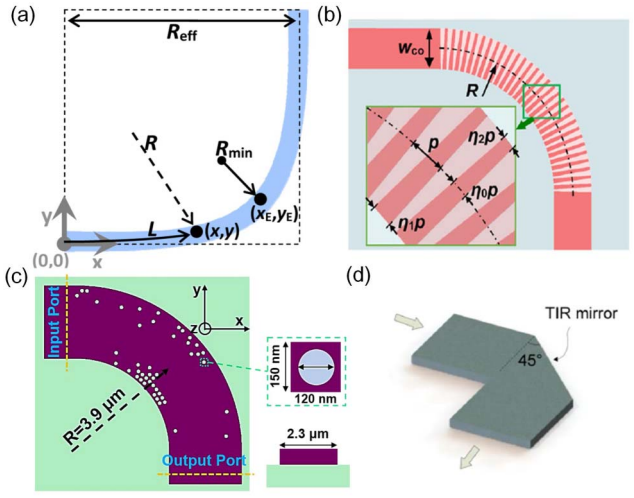

Fig. 4. Schematic diagram of integrated multimode waveguide bends: (a) the Euler curved bend for four TM modes[49], (b) the dual-mode bend with MC[54], (c) the pixelated four-mode bend structure[51], (d) four-mode bend based on a TIR mirror[56].

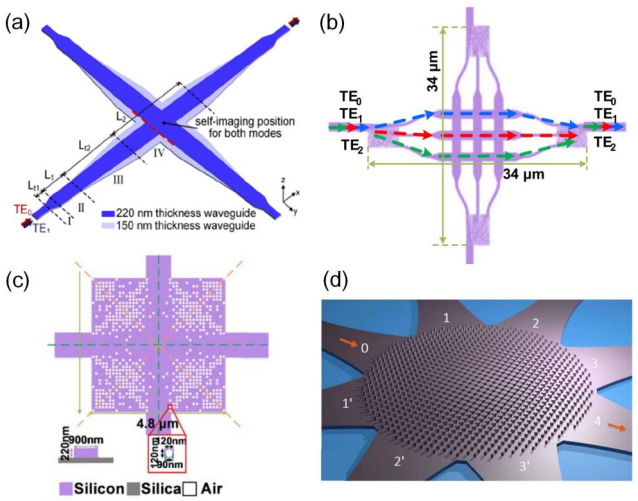

Fig. 5. Schematic diagram of integrated multimode waveguide crossing: (a) two-mode crossing based on non-adiabatic tapered waveguide[58], (b) three-mode crossing based on pixelated mode MUX and single-mode crossing array[60], (c) ultra-compact multimode crossing for two TE modes[61], (d) meta-material-based dual-mode star-crossing[62].

even shorter bends can be obtained for multiple modes. By adding a subwavelength grating in the bending region, six modes with dual polarizations can be bent by the 10 μm radius with loss under 0.23 dB in a wide range of 100 nm[50].

Thirdly, in recent years, inverse design has become a novel design method for PIC devices, in virtue of the ability to break the conventional design frame and automatically obtain the optimized devices with outstanding performance and compact footprint. Ultra-compact multimode bent waveguides can be optimized based on pixelated meta-structures, with a 3.6 μm radius and <1 dB loss for two TE modes[55] and for four TE modes[51] [in Fig. 4(c)]. The inversely designed multimode bend is more suitable for high-density MDM systems despite a slightly higher bending loss, while the two kinds of multimode bends mentioned before have more benefits in the loss-sensitive MDM system with less demand on compactness.

Furthermore, inspired by the on-chip-geometrical-optics configuration, a novel four-mode bend based on a total-internal-reflection (TIR) mirror was reported in Ref. [56], as shown in Fig. 4(d). The same concept was also used for the MDM crossing, 3 dB coupler, and switch, with easy design and scalability to much larger mode numbers. However, these four-mode devices are constituted by a 10-μm-wide waveguide, which still needs a long adiabatic taper to match with normal four-mode waveguides.

Crossing is another basic component in high-density MDM networks. Seeing that the conventional single-mode waveguide crossing is typically based on the self-imaging of multimode interference (MMI), the multimode waveguide crossing can be designed by the same principle. Dual-mode crossing was proposed by optimizing the joint self-images of two TM modes[57] and two TE modes[58] under the footprint around 30 μm × 30 μm, as shown in Fig. 5(a). Another method is to divide or convert the HOMs into the fundamental mode, set an array of single-mode crossings, and then combine or reconvert them into HOMs[59]. In view of that, a three-mode waveguide crossing was demonstrated in a 34 μm × 34 μm footprint, with 0.9 dB insertion loss and −22 dB crosstalk[60], seen from Fig. 5(b). Besides, the inverse design method can also be applied to optimize an ultra-compact multimode crossing, and dual-mode crossing was achieved in an ultra-small size of 4.8 μm × 4.8 μm[61], as depicted in Fig. 5(c). Furthermore, meta-material-based dual-mode star-crossing was presented in Ref. [62], showing four-channel crossing for two TM modes with <0.3 dB loss, <−20 dB crosstalk, and an 18 μm × 18 μm footprint [Fig. 5(d)].

2.3.2. Power coupling devices

In an MDM photonic integrated system, a power splitter is the basic component to allocate the power distribution of multi-mode signals in different channels. A dual-mode 3 dB power splitter was designed by a straightforward structure[63]. The guided modes in multimode waveguides are demultiplexed, converted to odd-order modes, which have an even number of lobes, and sent into a symmetric Y junction to be split by a 50:50 power ratio. While such design is not size-efficient, it can easily scale up the mode order. A directional coupler (DC) is a common structure for power coupling, with an arbitrary splitting ratio under different coupling lengths. Based on that, an asymmetric tapered DC was proposed as a 3 dB power splitter for two TM modes[64]. However, the 50:50 power ratio cannot be satisfied for both modes over a broad wavelength range. Besides, an ultra-broadband 3 dB power splitter for four modes was reported based on an adiabatic coupler and a Y branch[65], but the total length of 800 μm depressed its practicability. In order to fabricate a multi-mode 3 dB power splitter with a compact footprint, broad

bandwidth, and scalability to more mode orders, an inverse design provides a new route to maintain all of the properties mentioned above. The 3 dB power splitters based on subwavelength pixelated structures were inversely designed for 2 and 3 TE modes, with compact sizes of $2.88\,\mu m \times 2.88\,\mu m$ and $4\,\mu m \times 4.5\,\mu m$, respectively[66,67]. It also has the potential to realize multimode power splitters with various ratios.

2.3.3. Mode manipulation devices: MUX/deMUX/mode converter/exchange/filter

Mode MUXs/deMUXs are the most significant devices in MDM systems, where they convert the different channels of the fundamental mode to HOMs, combine them together in multimode waveguide channels, and finally reconvert the HOMs to fundamental modes and separate into the original channels. For photonic integrated MDM systems, mode MUXs/deMUXs have already attracted plenty of researches in recent decades. Till now, the structure of the mode MUX/deMUX can be classified into plenty of types, such as MMI[9,68,69], DCs[12,15,70–72], Y junctions[73–76], micro-rings[77–80], grating-assisted structures[81–83], and inversely designed structures[84–86]. Table 4 lists the mode MUXs based on various structures and their performances.

First, the MMI-based mode MUX typically presents wide bandwidth and high tolerance to fabrication errors with a long

Table 4. The Summary of Mode MUX/deMUX.

Ref.	Year	L (μm)	IL_{max} (dB)	CT_{max} (dB)	BW (nm)	Channel	Structure	E / S[a]
[9]	2012	80	1	−40	50	2 (TE)	MMI + PS	S
[68]	2014	48.8	0.3	−22	100	2 (TE)	Symmetric Y junction + PS + MMI	S
[69]	2020	7.24	0.74–1.2	−15	50	2 (TE)	Shallow-etched MMI	E
[70]	2013	50	0.3	−16	100	2 (TE)	Adiabatic tapered ADC	E
[72]	2016	68	0.8–1.3	−26	65	2 (TE)	Taper-etched ADC	E
[15]	2018	15–50	0.2–1.8	−15 to −25	90	10 (PM)	Adiabatic tapered ADC	E
[71]	2019	75	1.5	/	75	12 (TE)	Adiabatic ADC using SWG	E
[73]	2013	~1000	1.5	−9	100	2 (TE)	Asymmetric Y junction	E
[74]	2016	510	5.7	−9.7 to −31.5	29	3 (TE)	Cascaded asymmetric Y junction	E
[12]	2013	300	0.3	−36	100	2 (TE)	Adiabatic coupler	E
[75]	2016	200	1	−20	75	2 (TE)	Adiabatic coupler + Y junction	E
[76]	2017	180	1.5	−19	90	2 (TE)	Adiabatic coupler + Y junction	E
[77]	2014	25	3–16	−12 to −22	/	3 (TE)	Micro-ring	E
[78]	2015	100	1.5–3.5	−20 to −32	/	3 (TE)	Micro-ring	E
[79]	2019	40	2.1	−19.7	/	4 (TE)	Micro-ring	E
[81]	2013	90–250	0.2–0.34	−22 to −30	3.7–11.8	4 (TE)	Grating-assisted contra-DC	S
[82]	2015	/	/	−22	/	2 (TE)	Grating-assisted tapered contra-DC	E
[83]	2020	300	6.6	−18.7	~4	4 (PM)	SWG-based contra-DC	E
[84]	2016	2.6×4.2	1.2	−12	100	2 (TE)	Topology optimized structure	E
[85]	2018	3.6×4.8	1.2–2.5	−19	60	3 (TE)	Pixelated structure	E
[86]	2020	5.4×6	1.5	−14.6	60	4 (TE)	Pixelated structure	E
[87]	2018	~1000	4	−13.7	40	2 (TE)	Triple waveguide coupler	E
[88]	2018	7.5	0.32	−15	35	2 (TM)	Triple waveguide coupler with hybrid plasmonic waveguide	S

[a]E, experimental result; S, simulation only.

size and becomes complicated for HOMs greater than the second one. However, an asymmetric shallow-etched MMI was reported as a two-mode MUX with a footprint of 1.5 μm × 7.24 μm[69], which is much shorter than the conventional MMI-based MUX, also having the potential for a higher-order mode MUX. Second, the most widely used mode MUX is based on an ADC in virtue of its broadband, simple design principle of phase matching, and high scalability by a cascaded ADC. Although the phase matching condition is highly sensitive to width variation of the fabricated waveguide, it can be improved by applying the adiabatic tapered ADC for mode MUX[70] so as to increase the fabrication tolerance and reliability. Based on the cascaded adiabatic tapered ADC, the robust 10-channel MDM system with dual polarization was demonstrated on the SOI platform[15] [as depicted in Fig. 6(a)], showing low insertion loss, low crosstalk, and broad wavelength band of 90 nm, and highly expanding the total capacity of on-chip optical interconnection. Besides, an optimized adiabatic ADC using subwavelength waveguides (SWGs) was proposed for mode MUX up to the 12th HOM[71], which is the highest order of mode MUX currently. Furthermore, similar to the principle of ADC, a triple-waveguide coupler can also realize mode MUX with scalability[87]. With the combination of novel material, like phase-change material[89] or hybrid plasmonic waveguides[88], it can serve as a reconfigurable mode MUX or switch. Third, the Y junction is another simple design for mode MUX, as shown in Fig. 6(b). Theoretically, an asymmetric Y junction is able to achieve many HOMs[73,74,90] and can also be combined with adiabatic tapers[75–86]. Otherwise, it generally needs to be large scale with hundreds of micron, which is not suitable for compact systems. Fourth, a micro-ring-based mode MUX has the same principle as DC at the coupling region. The resonator structure is easily compatible with WDM[77,78] and is also applied to selective mode conversion, despite the narrow bandwidth in one wavelength channel. In addition, it is more convenient to combine signal modulation and mode MUX/deMUX together on a single micro-ring so as to achieve an ultra-compact on-chip MDM system[79], as shown in Fig. 6(c). Finally, the inverse design method brings a wider design space for mode MUX[84,85], which can obtain the ultra-compact footprint that the above-mentioned structures have no chance to reach. A four-mode MUX was optimized by a pixelated waveguide in Ref. [86] [shown in Fig. 6(d)] with a small size, broadband, and slightly higher insertion loss, and still scalable to other higher-order modes. By means of the inversely designed pixelated structure, the MDM circuit including mode MUX, multimode bends, and crossings was demonstrated in an ultra-compact size[91]. This work significantly improves the integration density on the dimensions of space and capacity.

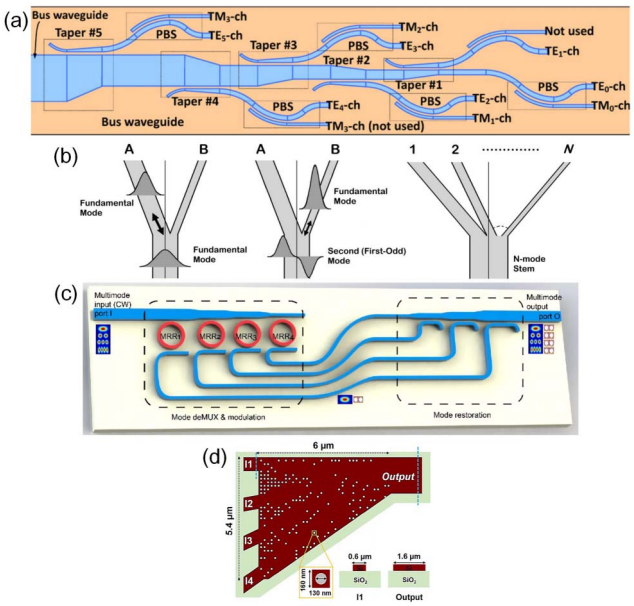

Fig. 6. Schematic diagram of integrated mode MUX/deMUX: (a) 10-channel mode (de)MUX with dual polarizations by adiabatic tapered ADC[15], (b) asymmetric Y-junction-based mode MUX[90], (c) MRRs serving as modulators and mode MUXs simultaneously[79], (d) four-mode MUX based on pixelated waveguides[86].

Besides the mode MUX/deMUX, the MC[92–96], mode exchange[97–99], and mode filter[100,101] have also been investigated recently for mode manipulation on the PIC. Here, the MC represents the device that can convert one input mode into another output mode at a single structure. A novel design combining the DC and slot-waveguide-based phase shifter for MCs from TE_0 to TE_1, TE_2, TE_3 was fabricated with compact size and low loss[93]. As shown in Fig. 7(a), a similar structure was designed to realize universal building blocks for arbitrary HOM conversion and exchange, and up to a 28th-order MC was demonstrated by simulation[94]. By means of an inversely designed pixelated structure, three-mode reflective converters[95] and two-channel parallel MCs[96] were presented for certain scenarios in the MDM system. In addition, mode exchange is used to exchange the signal between different mode channels, such as exchanging signals carried on the TE_0 and TE_1 modes[97]. With micro-ring-based mode MUX, the selective mode exchange between TE_0 and arbitrary HOMs was capable of thermally controlling the resonant wavelength[98]. As shown

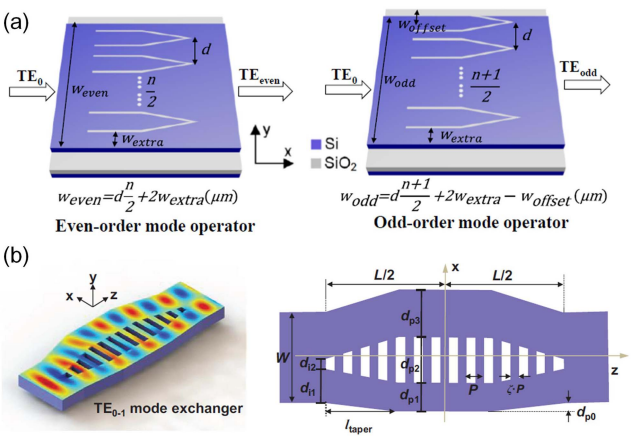

Fig. 7. Schematic diagram of universal (a) MC[94] and (b) mode exchanger[98].

in Fig. 7(b), ultra-compact and ultra-broadband mode exchangers were reported by SWG-based structures with universal practicability[99]. TE_{0-1} and TE_{0-2} mode exchangers with $<3\,\mu m$ length were fabricated for proof of concept. Ultimately, the mode filter can be employed to cut down the undesired mode and also to increase the mode crosstalk. A TE_1 HOM pass filter was presented by one-dimensional (1D) photonic crystal grating waveguides with compact size and broadband[100]. A reconfigurable mode filter or exchange was demonstrated in Ref. [101] for two TE modes.

2.3.4. Wavelength/polarization manipulation devices: filter/polarization splitter/rotator

As we reviewed before, passive multimode devices constitute the foundation of the integrated MDM system. At the same time, some multimode devices are capable of wavelength/polarization manipulation as well. For instance, ADC-based mode conversion can drop certain polarization modes so as to obtain the polarization splitter. Based on such a principle, a polarization beam splitter (PBS) was reported in Ref. [102], in which the TE_0 mode is dropped down from TM_0 by converting into the TE_1 mode through ADC-based mode MUX and then coupling back to TE_0 through another ADC, as shown in Fig. 8(a). Besides, another PBS was composed by an ADC-based mode MUX and multimode asymmetric sidewall Bragg grating[103]. As depicted in Fig. 8(b), gratings on the two sides have half-of-period offset along the propagation direction, resulting in π phase difference, which presents the contra-DC between TE_0 and TE_1. Thus, the input TE_0 is reflectively coupled into TE_1 and dropped down through the ADC mode MUX. The same principle is also applied for the wavelength filter. The wavelength range that satisfies the phase matching condition in contra-DC will be filtered back and dropped off by mode MUX[104]. The lateral-apodized shift between two gratings was employed to suppress the strong side lobes of the filtered spectrum[105]. By means of multiple mode MUXs and even multiple multimode asymmetric gratings, the structure can be used for an add-drop filter[106], with a tunable spectrum as well[107]. Furthermore, a polarization rotator (PR)[108] and a polarization splitter rotator[109] were demonstrated by multimode waveguide coupling as well.

As mentioned before, inspired by an on-chip-geometrical-optics configuration, multimode bend, crossing, 3 dB coupler, and switch were demonstrated by a TIR mirror, which provides a brand-new concept for designing multimode devices. Besides, the TIR mirror was also applied to realize a mode-transparent PBS in a wide multimode waveguide, as depicted in Fig. 8(c). PBSs for 13 modes, including six TE modes and five TM modes, were demonstrated with low insertion loss and low modal/polarization crosstalk[110].

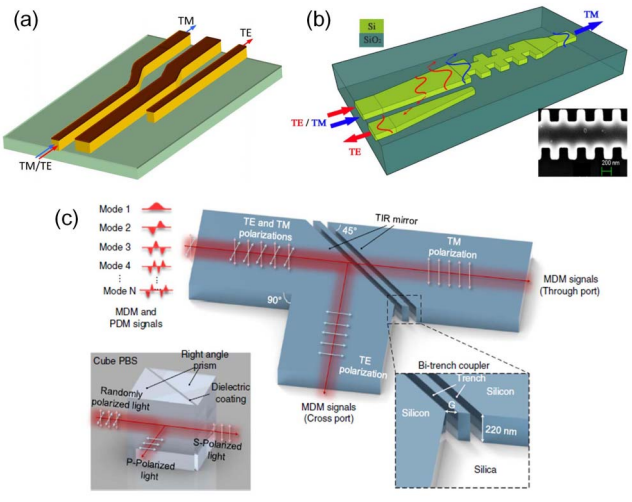

Fig. 8. Schematic diagram of (a), (b) integrated PBS based on mode conversion[102,103] and (c) mode-transparent PBS based on TIR mirror[110].

2.4. Active devices

2.4.1. Modulator

In the MDM photonic integration system, different spatial modes should be sent into different modulators separately and then combined by mode MUX for MDM transmission. Here, each mode is treated as an independent channel and modulated by an independent electric signal. As a result, there is not any multimode modulator that supports the multimode transmission and EO modulation at the same time. However, the working principle of MDM could also be utilized in the integrated modulator to improve the performance in size and modulation efficiency. For instance, in Ref. [111], Zhou *et al.* demonstrated a Si-based modulator, which was composed of the multimode waveguide as phase shifter, as shown in Fig. 9(a). Different from the traditional Mach–Zehnder interferometer (MZI), this type of phase shifter has only one arm. Two branches of light travel as different spatial modes, TE_0 and TE_1, and finally interfere with each other at the output port. This type of modulator reduces one arm in the MZI interferometer, thus reducing the optical device size by half. On-off keying modulation was demonstrated with extinction ratio of 5.5 dB at 32 Gb/s.

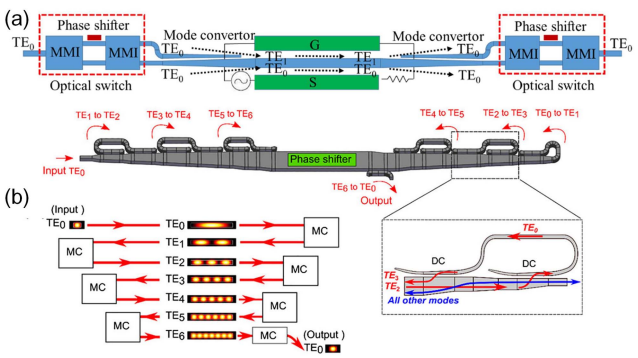

Fig. 9. Schematic diagram of (a) Si-based MZI modulator with two branches of light propagating in one multimode waveguide[112], and (b) spatial mode recycling scheme used to reduce the required power consumption[113].

Besides, the orthogonality among different spatial modes allows them to share one physical channel simultaneously.

Reference [113] shows that different spatial modes could go through one phase shifter successively, thus increasing the effective optical length. As shown in Fig. 9(b), the thermal-optic phase shifter consists of a multimode waveguide and several MCs based on the DC structure. In the recycling structure, light is input as the TE_0 mode at first, then converts into the TE_1 mode via two mode MUXs at the end of the phase shifter, and is sent back to the bus waveguide in the opposite direction. After going through the phase shifter two times, it is then converted to the TE_2 mode and sent back to the bus waveguide in the forward direction. By recycling the light in the bus waveguide for n times, the phase change enlarges n times accordingly. The thermo-optic phase shifter finally realized the power consumption of 1.7 mW per π, which is more than an eight-time reduction compared with the traditional MZI structure. Notably, the light recycling scheme makes a difference on the phase shifter based on the thermo-optic effect; that is because the efficiency of thermal tuning for HOMs does not decrease as the waveguide grows wider, while totally differing from the multimode phase shifter based on the carrier dispersion effect. The low-energy phase shifter makes a great difference for the optical phased array and Lidar applications, which will be discussed in the next section.

2.4.2. Switch

Different from the MC, which is used to convert spatial modes to each other, a typical mode switch should be able to support data exchange between any two spatial modes that carry different transmission data. In Ref. [114], a simple MC can be realized by combining two uniform MCs together, as shown in Fig. 10(a). Two micro-ring-based MCs that convert the TE_0 mode to the TE_1 mode were combined. When the input is the TE_0 mode, it will go through the MRR1, couple in MRR2, and then convert to the TE_1 mode. Similarly, when the input is the TE_1 mode, it will couple in MRR1, convert to the TE_0 mode, and then go through MRR2. In Ref. [115], a reconfigurable mode switch based on the MZI structure was proposed by Sun *et al.* The schematic of the proposed structure is shown in Fig. 10(b); the whole structure consists of two symmetric Y junctions and a phase shifter. The input TE_0 mode will evolve first into an even super-mode and then split to two branches with uniform optical phase. Similarly, the input TE_1 mode will evolve into an odd super-mode and then split to two branches with opposite optical phases. When the state of the switch is OFF, the two branches of light will arrive at the output port without any change. When the state of the switch is ON, the upper branch of light will be induced to a π shift, and thus the output mode will be changed.

A similar concept was also used for high-speed two-mode switches based on a Y junction, phase shifter, and MMI[116]. However, such a design is only suitable for a two-mode switch. The mode switch among different modes becomes more complicated and more difficult to realize as the mode number increases. Jia *et al.* demonstrated a passive multimode switch by inversely designed subwavelength meta-structures[117]. The transmitted four modes TE_0, TE_1, TE_2, and TE_3 are converted to TE_2, TE_0, TE_3, and TE_1 in a multi-functional device with a footprint cost of 4 μm × 3.4 μm. Such a design can realize multiple switch functions in a single and compact device but can hardly be reconfigurable. As we mentioned before, inspired by geometrical optics, a multimode 3 dB coupler can be made by a narrow trench. By means of such a multimode 3 dB coupler, a multimode thermal switch was reported, as depicted in Fig. 10(c)[56]. The multimode switch is based on the conventional MZI structure with a 10-μm-wide multimode waveguide. No matter, the narrowly trenched 3 dB coupler, or the thermal phase shifter, can be scaled up to even more modes. Multiple modes must be routed at the same time, and the measured extinction ratio is not competitive. Over all, a reconfigurable multimode switch holding more than two modes is still a challenging objective. With the help of the subwavelength adiabatic multimode Y junctions[118], the reconfigurable mode switch may have more potential to realize more modes.

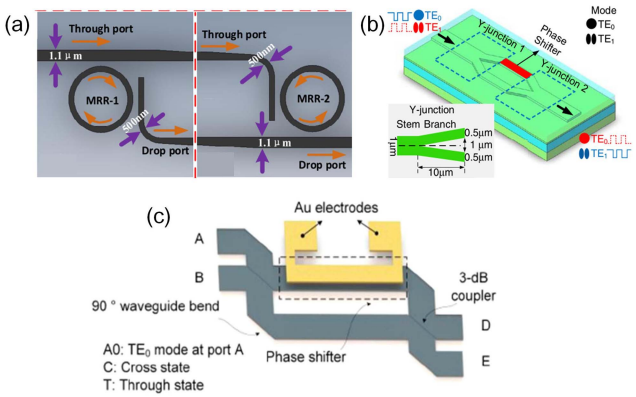

Fig. 10. Schematic of (a) mode switch based on two micro-rings[114] and (b) reconfigurable mode switch based on an MZI structure[115]. (c) Four-mode thermal switch by geometric-optic inspired multimode 3 dB coupler[56].

2.5. MDM circuits and subsystems

Based on the fundamental passive multimode devices introduced above, large-scale MDM circuits and subsystems can be built for various functions, like switching and routing. Besides, other functional devices or systems can also be innovated by means of the concept of MDM with high-efficiency spatial utilization, for instance, the optical phased array. In this section, we will list some large-scale reconfigurable optical integrated MDM systems for switching, routing, and even phase controlling and discuss their prospect and challenges.

2.5.1. MDM for optical phased array

Optical phased array provides a prospective solution for beam-steering applications in ultra-small solid-state Lidar and free-space communication systems. For the large-scale optical phased array, power consumption is an intractable problem,

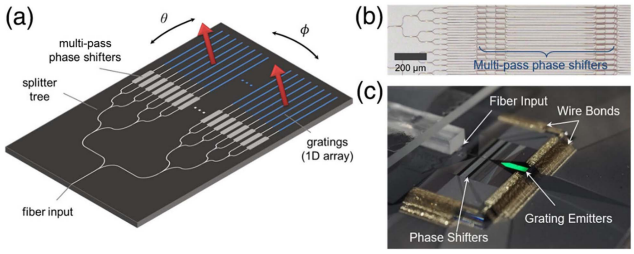

Fig. 11. Schematic diagram of Si optical phased array based on multi-pass recycling structure by mode multiplexing[119].

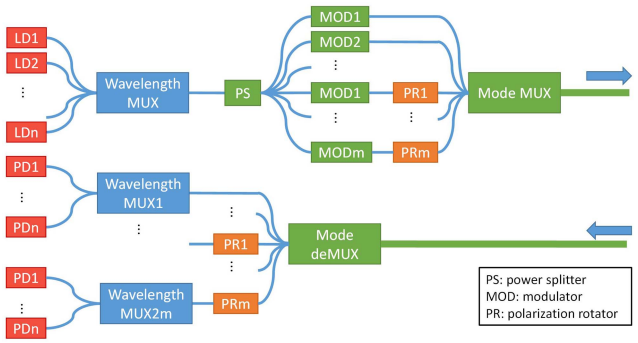

Fig. 12. Schematic diagram of integrated interconnect system hybrid multiplexed by WDM, MDM, and PDM.

since the thermal-optic phase shifter typically consumes tens of milliwatts of power and results in an overall power consumption of hundreds of watts. To solve that problem, Miller *et al.* demonstrated a high-efficiency large-scale Si integrated optical phased array using an MDM-based multi-pass phase shifter, as shown in Fig. 11, totally containing 512 actively controlled elements and consuming only 1.9 W of power while performing 2D beam steering over a $70° \times 6°$ field of view[119]. The multi-pass phase shifter consists of seven adiabatic tapered ADC-based mode MUXs to convert the input fundamental mode TE_0 into six HOMs (TE_1–TE_6) in sequence and finally reconvert to TE_0 as the output. The multiple orthogonal spatial modes circulate through the same phase shifter without any undesired interference, and optical phase is accumulated during the recycling. Thus, the multi-pass phase shifter consumes only 1.7 mW of power for the π phase shift, which is reduced by nearly nine times compared with the conventional one-pass phase shifter. The reason why the reduction factor of power consumption is slightly higher than the number of passes is that HOMs present higher sensitivity to thermal variation as a result of stronger dispersion. The insertion loss of the seven-pass structure was 4.6 dB, which can be improved by optimizing the mode MUX. In general, the optical phased array based on MDM relieves the power-hungry problem to a great extent without satisfying the tuning speed and broadband operation and shows the prospect of large-scale integrated optical phased arrays with large range and low-power consumption.

2.5.2. MDM interconnect system (hybrid with WDM/PDM)

Multiplexing technology can generate tens or even hundreds of times of increased capacity of the overall interconnect system, especially by hybrid multiplexing of wavelength, space (mode), and polarization domains. In order to actualize hybrid multiplexing, MDM devices have to present broadband operation to satisfy as many wavelength channels as possible. Figure 12 illustrates the scheme of hybrid multiplexing, in which all of the elements except for the wavelength MUX have broadband operation containing the wavelength range of WDM. The WDM channels are combined by wavelength MUX, then split, and modulated to form MDM/PDM channels via the PR and mode MUX. The hybrid signals propagate in the multimode waveguide and are de-multiplexed in the reverse process. As a realized demonstration, 12 hybrid multiplexed channels ($4\,\text{WDM} \times 3\,\text{MDM}$) were reported on the MDM circuit by micro-ring-based mode MUX, with a single-channel speed of 10 Gb/s[78]. In addition, 10-channel mode MUX (containing PDM) was demonstrated in Ref. [15] and achieved 20×30 Gb/s total transmission with the help of two hybrid WDM channels. Actually, in the conventional C + L wave band, WDM is capable of providing nearly a hundred wavelength channels. As for the MDM devices we discussed above, the state-of-the-art mode number that is multiplexed in the multimode waveguide with low loss and low crosstalk can be up to 10[71]. Counting in the two polarization channels, the on-chip interconnect system can accommodate at least a thousand of multiplexed channels, achieving total information capacity of higher than 100 Tb/s in case of 100 Gb/s single-channel speed. As a result, there is a promising future for hybrid multiplexing technology in optical interconnection with ultra-high capacity[120], in which MDM circuits compatible with WDM occupy the significant status.

2.5.3. MDM switch network/ROADM system

Optical switching and reconfigurable optical add-drop multiplexing (ROADM) are vital functionalities for optical interconnect networks. Multiplexing technology like MDM and WDM increases the density and capacity of optical networks, while also bringing in the challenge of switching and ROADM. In recent years, reconfigurable switch arrays and ROADM for hybrid multiplexing systems have been investigated in various schemes. The majority of them are based on MUX/deMUX and conventional 2×2 single-mode switching units, that is to say, the multiplexed signals of each path are firstly demultiplexed into individual channels, then arrays of 2×2 switching units selectively route the signals among different channels and paths, and finally the reconfigured channels are again multiplexed into HOMs in original paths and output. The schematic process is illustrated in Fig. 13(a). For instance, Jia *et al.* reported the 2×2 WDM-compatible multimode switching circuits with all the optical network on-chip except for the WDM source[121]. Micro-ring arrays are employed as wavelength MUX/deMUX

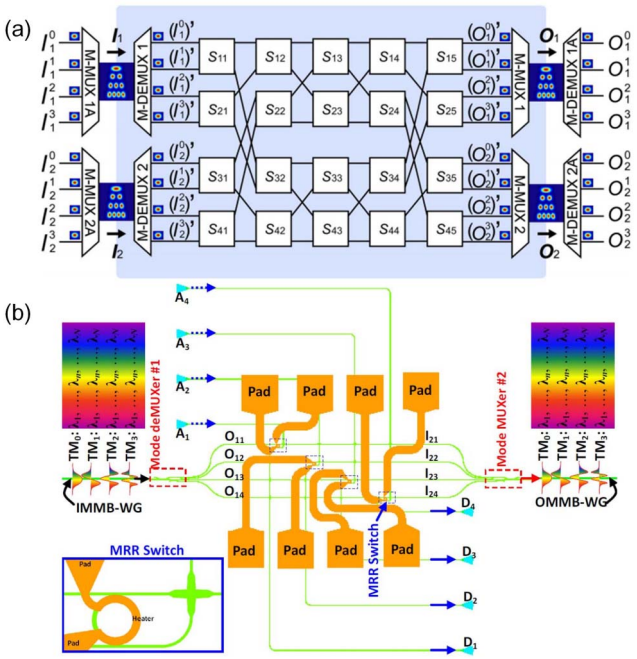

Fig. 13. Schematic diagram of on-chip switching networks ROADM for multiplexing: (a) on-chip typical multimode optical switching system[125], (b) on-chip ROADM system for hybrid WDM and MDM[129].

and modulators, and multimode switching consists of mode MUX/deMUX and single-mode switching units with broadband operation and WDM compatibility. As a proof of concept, they demonstrated the switching network along two multiplexed paths containing three wavelength channels and two mode channels, showing error-free switching of 25 Gb/s single-lane signals. There are also other hybrid multiplexed switching networks based on the same scheme[122–125]. However, the complexity, footprint, and power consumption of switch arrays rise sharply with the increasing numbers of multiplexed channels and paths. Sun *et al.* presented the multimode switch network by means of a novel structure, which is free from de-multiplexing and re-multiplexing operations and easily upgradable to a larger scale[126,127]. Every 2×2 switch unit for two TE modes consists of two Y junctions to split/combine the mode field into/from two lobes with in-phase or out-of-phase, two phase shifters to change the phase between two lobes, and two micro-rings with two coupling regions to selectively switch the path. Such a scheme is easier to scale up to the $N \times N$ dual-mode switching network with compact size; however, it is only suitable for dual-mode multiplexing systems and not for further higher-order modes. Besides, ROADMs for MDM systems are demonstrated by de-multiplexing, routing networks, and re-multiplexing operations[128] and are compatible with WDM as well[129,130], as shown in Fig. 13(b). Above all, the large-scale switching and ROADM system for multi-path, hybrid multi-channel multiplexing are still strongly desired for future high-capacity high-density optical multiplexing networks.

3. Large Capacity MDM Optical Fiber Transmission

3.1. FMF fibers

The FMF is the basic and essential part in MDM systems to enlarge the total capacity of fiber optic communication systems. Due to the modal coupling among different modes, MIMO is applied to recover signals that have been degraded during the FMF transmission and mode MUX/deMUX[131], which make the system more complex and time-consuming as the number of modes increases. This section will introduce recent researches on the fiber design of FMFs, mainly focusing on the structure to transmit more stable modes and reduce MIMO complexity.

3.1.1. Conventional FMF for MIMO-less MDM

The complexity of MIMO processing is mainly caused by large mode crosstalk and differential mode group delay (DMGD). Here, we introduce two kinds of FMFs to reduce mode crosstalk for MIMO-less MDM systems.

Firstly, step index fibers with a standard structure are proposed to reduce mode coupling by enlarging the effective index (n_{eff}) between mode groups. For instance, a four-LP-mode FMF with n_{eff} differences $\geq 0.8 \times 10^{-3}$, differential group delays (DGDs) of 1–9 ps/m, A_{eff} of 118–133 μm^2, mode-average loss <0.22 dB/km, and integrated crosstalk of -33 dB/km was designed, which can be used for three-mode transmission at 100 Gb/s over 40 km[132]. A seven-LP-mode fiber with a step index profile was fabricated with n_{eff} differences $\geq 0.9 \times 10^{-3}$ and crosstalk of -25 dB/km[133]. Meanwhile, as shown in Fig. 14(b), introducing a depressed zone in the center of the step core is an effective solution to increase n_{eff} differences ($\geq 1.6 \times 10^{-3}$) without deteriorating other characteristics (lossess <0.25 dB/km)[134]. However, it is difficult to enlarge the refractive index of higher-order modes with such a simple structure.

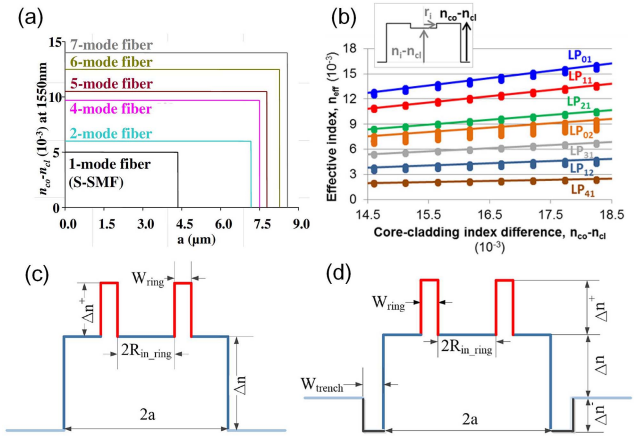

Fig. 14. (a) Optimized step-index profiles of different FMFs[133], (b) core-cladding difference for seven-LP-mode fibers with step-index and depressed-inner-core profiles[134], (c) refractive index profile of ring-assisted four-mode fiber[135], (d) refractive index profile of ring-assisted seven-LP-mode fiber with trench structure[136].

The second one is ring-assisted fibers with a multi-layer circle core and annular index structure providing more freedoms to enlarge Δn_{eff}. Jiang *et al.*[135] fabricated a mode ring-core fiber with optimized $\Delta n_{\text{eff}} \geq 1.8 \times 10^{-3}$ and average mode loss of 0.23 dB/km by adding an additional high-index ring [in Fig. 14(c)]. Although ring-assisted fibers show similar crosstalk with the step index fiber mentioned in experiments, they have better robustness to external fluctuation than step index fibers in practical applications, which is promising for the performance improvement of MUX and deMUX. To further improve the weak coupling performance, a low-index trench was introduced to ring-assisted fibers [in Fig. 14(d)] by considering the refractive index difference of trench-cladding, the width of the trench, and the distance of the core trench. Ma *et al.*[136] proposed a fiber supporting 12 spatial modes with $\Delta n_{\text{eff}} \geq 1.7 \times 10^{-3}$, effective area $\geq 103\ \mu m^2$, and loss of the LP_{22} mode $\geq$ 10dB/km at 1550 nm.

Thanks to these two fibers with lower mode coupling, the complex MIMO processing can be replaced by several simple local MIMO, eventually approaching MIMO-less. Besides, it is also desirable to simplify decoding complexity by lower DMGD, which compensates mode-coupling at the receiver side. In view of that, as seen from Fig. 15(a), Sato *et al.* fabricated a two-mode graded-index fiber with $\Delta = 0.363\%$ and $\alpha = 2.29$, which has a large effective area A_{eff} of 150 μm^2 for the LP_{01} mode and approximately 0.016 dB/km bending loss for the LP_{11} mode at $R = 40$ mm, and it realized differential mode delay (DMD) of <36 ps/km including zero in the C-band[137]. In addition, as shown in Fig. 15(b), a nine-LP-mode fiber with trench-assisted graded-index-core profiles was fabricated realizing DMGDs <155 ps/km at 1550 nm[138].

Another method to simplify or eliminate MIMO processing is employing elliptical core fibers by dividing different modes in the same degenerate mode group. This fiber is widely applied

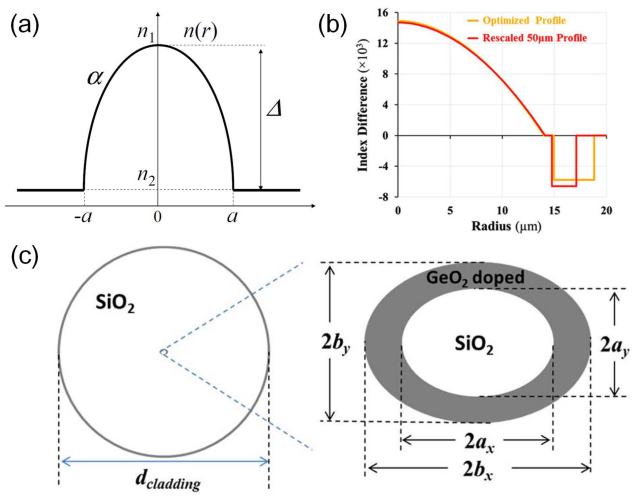

Fig. 15. (a) Refractive index profile of two-mode graded-index fiber[137], (b) refractive index profile of nine-mode graded-index fiber with trench-assisted structure[138], (c) geometry and parameter definitions of the elliptical core fiber[142].

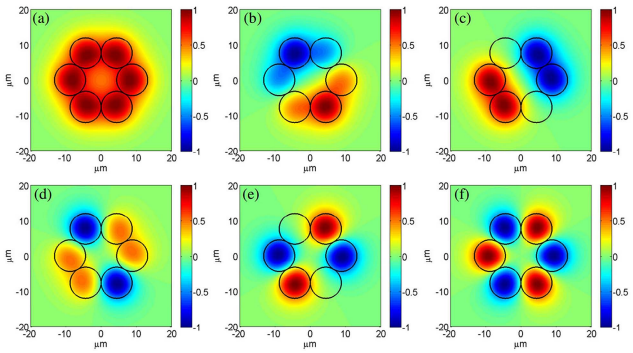

Fig. 16. Schematic of a multi-core super-mode fiber[143].

to a polarization-maintaining fiber (PMF), acousto-optic frequency shifters[139], inter-modal couplers[140], and spatial mode filters. In MIMO-less space division multiplex transmission at 1550 nm over 1 km, an elliptical-core FMF has been demonstrated to support the LP_{01},LP_{11a}, and LP_{11b} modes with low levels of modal crosstalk below −22 dB[141]. Wang *et al.*[142] designed a polarization-maintaining (PM)-FMF supporting 10 polarization and spatial modes with relatively small group velocity dispersions (GVDs) (−25 to 3 $ps \cdot km^{-1} \cdot nm^{-1}$), which can maintain both their polarization states and spatial orientations after a transmission of up to several hundred meters.

Furthermore, in recent years, multi-core super-mode fibers have been proposed as one of the important methods to increase the transmission capacity of long-distance MDM systems. Super-mode fibers can achieve higher mode density, higher design freedom, no mode-related loss, and larger effective area than single-core FMFs[143], as shown in Fig. 16. Considering that, a PM super-mode fiber supporting 20 modes was designed with Δn_{eff} among arbitrary modes higher than 10^{-4} and relatively larger A_{eff} than 47.67 μm^2[144].

3.1.2. Inverse design of FMF fiber

Conventional FMFs are based on sweeping the structure parameters to meet different characteristic requirements, which is time-consuming. Recently, an inverse design using neural network (NN) has been proposed with high accuracy, high efficiency, and low complexity for a fast and reusable design of optical fibers.

As shown in Fig. 17(a), the entire design process can be divided into two modules, forward design and inverse design. Forward design is utilized to generate a data set in different structure parameters by software simulation (like Lumerical or COMSOL). The inverse design process using NN is to automatically establish the mapping between the input and output from forward design by adjusting the weight of different layers and reducing error values. This inverse method is firstly used to design a weakly coupled fiber with a multi-ring structure supporting more modes. In Ref. [145], a sequential model with three hidden layers, where each layer has 300 neurons, was constructed to predict structure parameters of four-ring fibers supporting four modes with Δn_{eff} distribution meeting the weakly

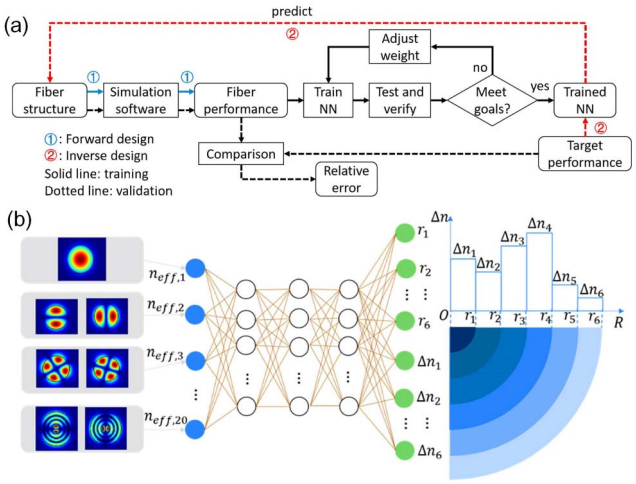

Fig. 17. (a) Flow chart of the proposed NN-assisted inverse design method. (b) The inverse design frame of the NN[145].

coupled objective. By comparing Δn_{eff} simulated by predicted parameters and target Δn_{eff}, the correlation of Δn_{eff} for all modes is above 0.99, and relative errors are below 0.0025%. In this way, we have successfully designed an FMF structure with a little larger maximum $\Delta n_{\text{eff, min}} (> 1.24 \times 10^{-3})$ in the initial data set. This proposed method will play an important role in the inverse design of other kinds of FMFs thanks to its good accuracy and low complexity.

3.2. MDM MUX/deMUX

In MDM fiber optic transmission systems, the transmitter generates multiple channels of fundamental mode LP_{01} into SMFs carrying different signals. In order to utilize the modes of FMF as independent channels, the signals of the LP_{01} mode need to be converted into higher-order modes and then multiplexed into the FMF. At the receiver, the multiplexed signals also need to be demultiplexed and then processed separately. Therefore, the MC and MUX are the fundamental devices in MDM systems. In particular, the MC and MUX are always realized by a single device, and we call it a mode MUX. Here, we introduce two main types of mode MUXs in fiber MDM systems: free-space beam MUX and all-fiber MUX.

3.2.1. Free-space beam multiplexer

Free-space beam MUXs change the optical field distribution of the fundamental mode to that of a higher-order mode by using a spatial light modulator (SLM)[146] or phase plate[147], which can achieve mode converting. As shown in Fig. 18, these optical beams of different modes are multiplexed by beam splitters (BSs). The SLM employs liquid crystal on Si (LCoS) technology to modulate the phase of beams, which is programmable and reconfigurable. Although the phase plate is simple and cost-effective, it must be specially designed for different modes. In early MDM systems experiments, free-space beam MUXs are widely used. However, its spatial light structure is incompatible

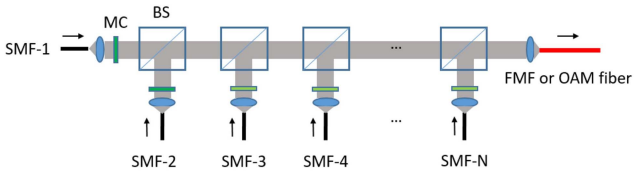

Fig. 18. Schematic diagram of mode MUX based on free-space beam combiner[148].

with fiber systems. This kind of mode MUXs needs optical systems with high complexity, stability, and precision. Moreover, the number of BSs increases with the number of modes, which will induce high insertion loss and thus limit the mode scalability of MDM systems. Therefore, although the free-space beam MUX has advantages on mode selectivity, mode crosstalk, and mode purity, it is not suitable for commercial systems.

3.2.2. All-fiber multiplexer

Since free-space beam MUXs use lenses to couple the light into the fiber, the coupling efficiency is quite low. In order to realize high coupling efficiency between MUXs and fibers, all-fiber MUXs are developed. There are three types of all-fiber MUXs: directional fiber coupler, long-period fiber Bragg grating (LPFBG) structure, and photonic lantern.

The directional fiber coupler can be achieved by a mode-selective coupler (MSC), which consists of one FMF arm and one SMF arm, as shown in Fig. 19[149]. The phase matching condition, $\beta_{01}^{\text{SMF}} = \beta_{\text{lm}}^{\text{FMF}}$, is required, where β_{01}^{SMF} and $\beta_{\text{lm}}^{\text{FMF}}$ represent the propagation constant of the LP_{01} mode in the SMF and the LP_{lm} mode in the FMF, respectively. The LP_{01} mode in the SMF is converted into the corresponding LP_{lm} mode in the FMF, and thus multiplexed into the FMF by the MSC. The MSC can be fabricated based on the polished fiber coupler or fused fiber coupler. Figure 19 shows the MUX and deMUX based on the directional fiber coupler supporting the LP_{01}, LP_{11a}, and LP_{11b} modes, which consist of two cascade MSCs.

LPFBG-based MUXs use LPFBG to realize mode conversion and use an FMF coupler to achieve multiplexing[150]. The

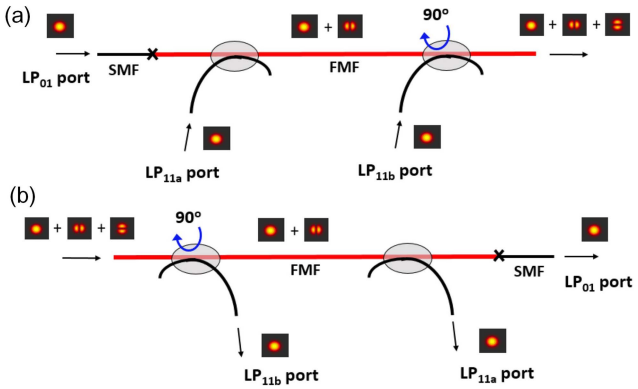

Fig. 19. Directional fiber-coupler-based (a) mode MUX and (b) mode deMUX supporting LP_{01}, LP_{11a}, and LP_{11b} modes[148].

LPFBG serves as an MC, as shown in Fig. 20. When the LPFBG meets the condition $n_1 = n_2 + \frac{\lambda}{\Lambda}$, where n_1 and n_2 are the effective indices of the LP_{01} mode and target LP_{lm} mode, respectively, the LP_{01} mode will be converted into the co-propagating LP_{lm} mode. The FMF couplers are made of two identical FMFs. Figure 20 shows the LPFBG-based MUX and deMUX supporting the LP_{01} and LP_{11} modes. A lobe orientation controller is employed to maintain mode orthogonality.

The two types of all-fiber MUXs from above achieve high coupling efficiency, but they lack flexibility. If the number of channels is increased, we need to add corresponding couplers into the MUX. Moreover, different modes are multiplexed or demultiplexed in order from the fundamental mode to the high-order mode. These disadvantages make it inconvenient for system building. Therefore, photonic lanterns attract the attention of researchers.

Photonic lanterns are an optical waveguide coupling light from several SMFs to one multimode fiber (MMF)[151]. A bundle of SMFs is inserted into a glass capillary tube with a low index. Then, by fusing and tapering down the tube, an all-solid MMF is formed at the other end, as shown in Fig. 21. For a traditional photonics lantern, each SMF in the bundle is identical, and the photonic lantern is not mode selective. When light is launched into one arbitrary SMF, the MMF will output all the modes. This kind of photonics lantern cannot control mode converting selectively; thus, the specific mode cannot be obtained dependently. Therefore, a traditional photonics lantern is unable to be utilized in MDM systems. Fontaine *et al.*, for the first time, to the best of our knowledge, analyzed mode converting in the photonics lantern by modal analysis, beam propagation, and transfer matrix[152]. They optimized each SMF and their geometrical arrangement to realize a mode-selective photonics lantern. Light launched into a specific SMF is converted into a corresponding high-order mode with low coupling loss and low mode dependent loss (MDL). These mode-selective photonics are widely used due to their simple structure, high integration, and high compatibility with WDM.

Fig. 20. LPFBG-based (a) mode MUX and (b) mode deMUX supporting LP_{01} and LP_{11a} modes. MC is achieved by LPFBG[148].

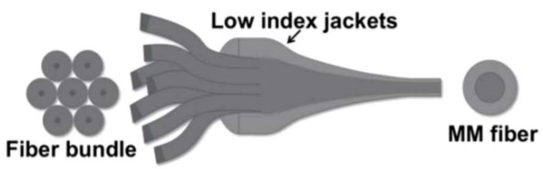

Fig. 21. Schematic diagram of a photonics lantern[151].

3.3. MDM amplifiers

In MDM transmission systems, amplifiers are a particularly important device due to the function of compensating the signal attenuation of fibers. Compared with amplifiers in SMF systems, besides conventional parameters of amplifiers such as gain and noise figure, we should also focus on the supporting modes and mode dependent gain (MDG) of MDM amplifiers. In MDM systems, the power difference of each mode should be controlled to be a low level, otherwise transmission performance will be reduced. Therefore, for MDM amplifiers, the gain difference between all modes, called MDG, must be small. Few-mode (FM) EDFAs and FM distributed Raman amplifiers (DRAs) are two widely adopted solutions, and they are developed from corresponding SMF amplifiers.

3.3.1. Few-mode erbium-doped fiber amplifiers

EDFAs are the conventional solution for light amplification in optical transmission systems, and they also can be extended into MDM systems. The main properties of FM-EDFAs are focused on the number of supporting modes, gain, MDG, noise figure, and so on. As single-mode EDFA has been extensively investigated, and the researches of FM-EDFAs are concentrated on the refractive index profiles and erbium doping profiles, which are effective solutions to reduce MDG.

The first proposed scheme is the design of erbium doping profiles. Jung fabricated a two-mode EDFA supporting LP_{01} and LP_{11} modes for the first time, to the best of our knowledge[153]. They doped erbium ions into the fiber core and made a higher erbium ion density at the edges of the core in order to achieve reduced pump field sensitivity for the modal gains. The two-mode EDFA realized the gain of 20 dB with an MDG of 5 dB. Furthermore, Fig. 22(a) shows a ring-shaped erbium

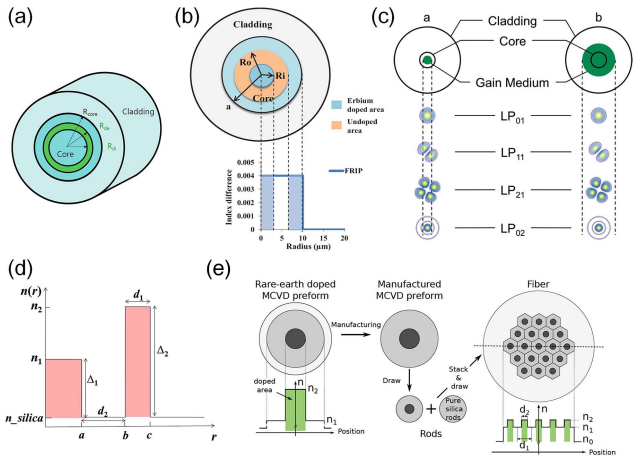

Fig. 22. (a) Ring-shaped erbium doping profile[154]. (b) Refractive index and doping profile (shaded region) of the four-mode EDF[155]. (c) Overlaps between mode fields and gain media in a small doped area (left) and a large doped area (right)[156]. (d) Schematic of dual-core fiber with dual-core doping and colored shadings representing erbium doping[157]. (e) Schematic description of microstructure[158].

doping profile in fiber core, which supports 4-mode EDFA and decreases the MDG down to 1 dB[154]. Kang extended the ring-shaped erbium doping profile and proposed central and ring-shaped erbium doping profile, as Fig. 22(b) shows[155]. In the simulation, this scheme supported four mode groups with 1 dB MDG. Considering HOMs have a larger mode field, which extend into the cladding, a large erbium-doped area over the core is needed to cover the field of all modes so that each mode can overlap with the erbium-doped area and get effectively amplified. For exciting erbium ions in the whole area, the cladding–pumping scheme is utilized. Based on this scheme, a four-mode EDFA was proposed, offering gain of more than 20 dB and MDG of less than 3.3 dB[156]. Refractive index profiles can also be combined with the erbium doping profile to further reduce MDG. As Fig. 22(d) illustrates, the fiber core was divided into three parts. The central part has a low refractive index and erbium doping. The middle ring has the same refractive index as the cladding and no erbium doping. The outer ring has a high refractive index and erbium doping. This scheme achieved the gain of 21 dB and MDG of 1.38 dB at the signal wavelength of 1530 nm. For the entire C-band, this scheme realized more than 21 dB gain and 1.75 dB gain excursion[157].

Precise distribution of the refractive index and erbium doping needs complex crafts, which makes the fabrication of erbium-doped fibers (EDFs) rather difficult. For solving this problem, an FM-EDF micro-structured with inclusions was reported[158]. As Fig. 22(e) displays, the fiber was made of 19 erbium-doped secondary cores embedded in a pedestal region and an optical cladding. This structure allowed for precise tailoring of the doping profile by using different homogeneously doped (or un-doped) preforms. The result showed that this structure supported five mode groups and provided average gain of 19.2 dB, a total gain excursion of 2.4 dB, and MDG of 1.1 dB.

3.3.2. Few-mode distributed Raman amplifiers

In MDM systems, as multi-channel signals are multiplexed and propagated together in the FMF, the power density will be much higher compared with SMFs, which lead to more serious nonlinear distortion. Moreover, crosstalk among different modes degrades the SNR of signals. In order to make full use of the limited bandwidth, advanced modulation formats, such as QAM, have been extensively investigated for increasing the spectral efficiency in SMF transmission systems[159]. MDM combined with advanced modulation formats would be an effective solution to further increase the capacity of MDM systems. However, advanced modulation formats require high SNR and better nonlinear performance. EDFA has a quantum-limited noise figure of 3 dB and serious nonlinear distortion due to the discrete amplification, as Fig. 23 shows[160]. Therefore, FM-DRAs are developed.

DRAs utilize stimulated Raman scattering to transfer the power from the pump to signal. DRA has many advantages compared with EDFAs. DRAs have higher SNR and less nonlinear distortion, as Fig. 23 displays. Moreover, DRAs have flexible gain profiles and bandwidth, which can be adjusted according

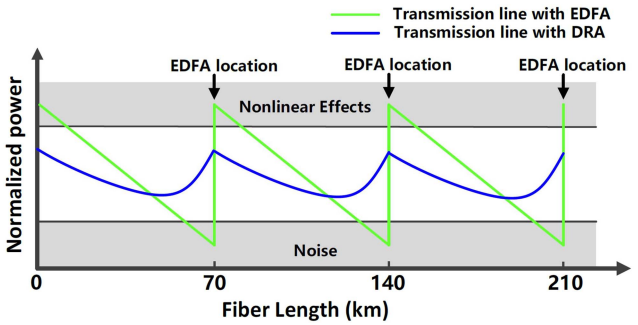

Fig. 23. Schematic principle of DRA for mitigating the nonlinear distortion and noise over EDFA[148].

to the demand by controlling the pump wavelength and power. MDG of FM-DRAs can also be controlled by customizing the pump component. Taking advantage of this merit, we can maintain the MDG of amplifiers at a low level or customize the MDG of amplifiers to compensate the MDL of the whole system. Finally, from the perspective of fabrication, DRAs only need several pump sources, while the manufacturing of EDFAs requires erbium doping according to a specific profile and drawing.

Ryf for the first time, to the best of our knowledge, demonstrated a backward FM-DRA supporting two modes[161]. In this work, they defined the intensity overlap integrals of two modes and gave the approximate amplification equations. Finally, they realized the gain of 8 dB with MDG of <0.5 dB. Esmaeelpour characterized the DRA in the 70 km three-spatial-mode fiber with different pump configurations, counter-pumping, co-pumping, and bidirectional pumping[162]. The bidirectional pumping FM-DRA was applied in the experiment of long-haul MDM transmission, and a signal was successfully transmitted over a distance of 1050 km, confirming that this distributed amplification scheme is suitable for long-distance transmission of SDM signals. Furthermore, Li experimentally demonstrated the MDM system with a flat gain two-mode FM-DRA covering 1530–1650 nm and induced 3.3 dB optical SNR (OSNR) enhancement[163].

DRAs for SMF systems have been widely investigated, and many novel structures are proposed to improve the performance. High-order Raman pumps can effectively improve the noise figure, thus being induced into MDM systems, with 1.8 dB improvement of amplified spontaneous emission (ASE) noise[164,165]. Moreover, equalized amplification in time and wavelength domains leads to the balance between noise and nonlinearity, like a quasi-lossless transmission link, as shown in Fig. 24[166]. DRAs have the capability to reduce the signal power variation (SPV) due to distributed structures, as compared to other discrete amplification such as EDFA. However, DRAs introduce the relative intensity noise (RIN), which is brought by the RIN of pump lasers[167]. The backward pumping scheme can effectively reduce the RIN, but it leads to a high SPV, because backward pumping can only provide amplification for the signal at the back of fiber due to the power attenuation of pumps. To further improve the noise performance of DRAs

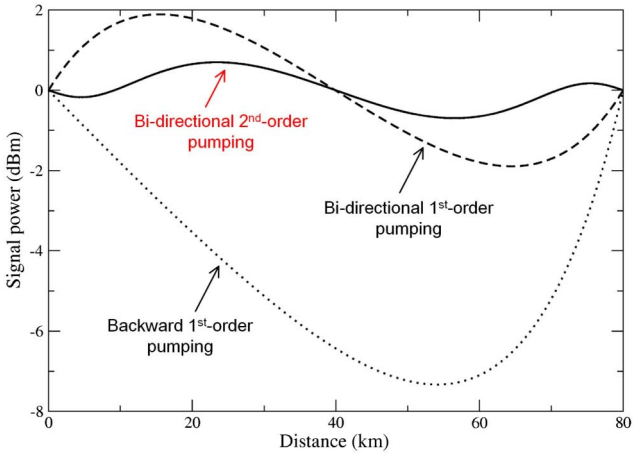

Fig. 24. Quasi-lossless transmission with bidirectional high-order pump[166].

and reduce the SPV, several schemes have been proposed in SMF systems. The second-order pumping scheme is an effective solution to enhance the performance of DRAs, which has been confirmed experimentally. A powerful scheme is based on a bidirectional pumping random fiber laser structure[167]. A single fiber Bragg grating (FBG) is put at the output port of the fiber, where the first-order Raman laser is reflected. Then, the backward second-order pump amplifies the reflected first-order pump. Since it is able to provide the amplification for the signal at the front and back of fiber, SPV can be effectively reduced. This scheme shows improved RIN performance compared to backward pumping only. Moreover, this scheme offers lower SPV due to the bidirectional pumping scheme, which will provide better SNR property and reduced nonlinear distortion.

For MDM systems, two algorithms for designing the FM-DRAs based on bidirectional pumping random fiber lasers were proposed. One of them was particle swarm optimization (PSO) for time, wavelength, and mode equalized FM-DRAs, which utilized four first-order pumps and one second-order pump[168]. Pump power was optimized by PSO to simultaneously minimize SPV, gain flatness, and MDG. Gain flatness of 1.5 dB, MDG of 0.03 dB, and SPV of 2.3 dB at 15 dB on–off gain were achieved. The other algorithm was a machine-learning-based inverse design[169,170]. Since obtaining numeral solutions of DRA is quite complex, an NN was used as an approximate mapping between gain profile and pump configuration. After being NN trained, an optimal pump configuration could be obtained by inputting the target gain profile into the NN. The inverse design based on NN is presented in Fig. 25, which consists of three processes: establishment of the NN, training, and validation. The utilized NN is a dense NN with four hidden layers and 500 neurons in each hidden layer. The data set for training is generated by equation solving with random pump parameters. Once the NN is trained, the reliability of the NN on the data out of the training set should be validated. The target gain spectra are input into the trained NN, and then the obtained pump parameters are used to calculate the actual gain spectra by an equation solver. The error between the actual spectrum and target

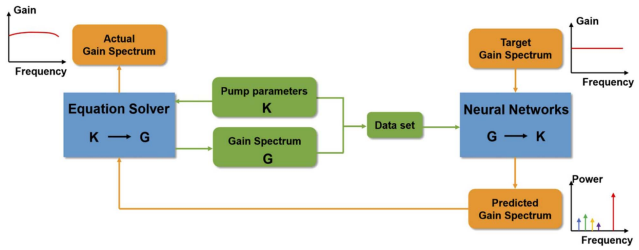

Fig. 25. Inverse design based on NN for FM-DRA[170].

spectrum is measured to evaluate the accuracy of the NN. By this method, they achieved 14.5 dB gain with gain flatness of 1.0 dB and MDG of 0.6 dB.

3.4. MDM transmission experiments and progresses

The research of MDM fiber transmission can be traced back to 1982 when two modes were transmitted over a 10 m MMF[171]. However, because of the limits of fiber fabrication, optical device, and DSP techniques, MDM did not attract much attention from researchers. In the 2000s, multimode amplifiers, MCs, and MUXs progressed, and MIMO technique were developed gradually, but high DMD of MMFs severely limited the performance of MDM systems. After the MMF was replaced by the FMF, MDM systems became achievable and were widely experimentally researched.

Current researches of MDM systems are mainly concentrated on the achievement of higher capacity and longer distance. The extension of capacity mainly depends on the number of channels, which is realized by increasing SDM channels and combining multiple hybrid multiplexing technologies such as WDM and PDM[172–175]. Ryf demonstrated 10-mode MDM transmission with 120 WDM channels over 121 km FMF with inline FM-EDFA, realizing the total capacity of 111.4 Tb/s and spectral efficiency of 29 bit·s^{-1}·Hz^{-1}[176]. Besides increasing the number of modes, combining MDM and multi-core multiplexing can also significantly increase the number of SDM channels[175,177]. Rademacher created a new capacity record of 10.66 Pb/s with three-mode 38-core fibers, realizing spectral efficiency of 1158.7 bit·s^{-1}·Hz^{-1}[8].

Compared with SMF systems, MDM technology induced MDL and DMD, which negatively affect the transmission distance. Rademacher demonstrated long-distance MDM transmission in three-mode fibers over 3500 km and gave the analysis of MDL that fundamentally limits the transmission reach[178]. The results indicated that MDL decreases the Q-factor of received signals, and it is continuously accumulated during fiber transmission, thus limiting the transmission distance of MDM. DMD is usually declined by low DMD fibers and DMD management technology such as DMD compensation fibers[179]. Moreover, cyclic mode permutation is proposed and utilized in DMD unmanaged long-haul SDM transmission[180,181]. Cyclic mode permutation is a technique to change the transmitted mode of the signal after propagating one span. For example, a signal is launched into the LP_{01} mode, and, after

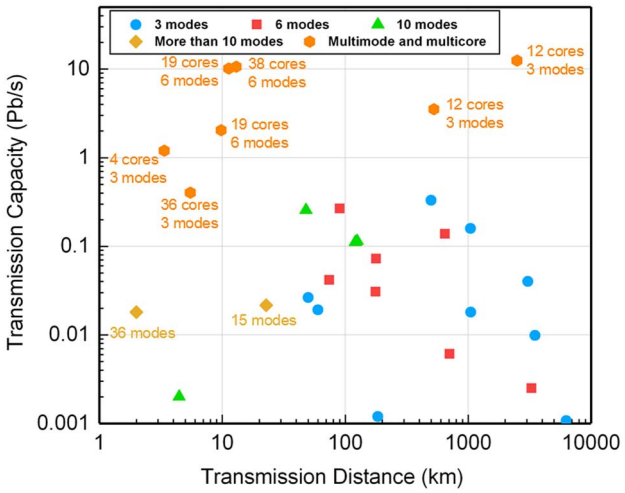

Fig. 26. Recent-year MDM experiments and progresses.

propagating one span, this signal is converted into the LP_{11a} mode. Then, this signal is converted into the LP_{11b} mode after the next span. This method makes all of the signals in different channels experience almost the same distance of each mode, effectively reducing DMD and MDL. By this technique, a record reach of 3250 km for six-mode MDM is achieved.

Figure 26 presents recent MDM experiments and progresses. Currently, large capacity and long distance are difficult to achieve at the same time, as large capacity demands more space modes but also induces MDL and DMD, which negatively influence the received signal. To further improve MDM systems for high capacity and long distance, besides developing the devices supporting more modes, MDL and DMD of MMFs are significant problems to be improved.

4. Conclusion

In this paper, we review the cutting-edge progresses of MDM technology for the scenerios from photonic integrated interconnection to optical fiber communication. Achievements of passive and active devices and MDM systems are summed up and discussed.

For MDM photonic integration, we give a review of integrated platforms, multimode interfaces for chip-to-fiber coupling, multimode passive devices (including bends, crossings, power splitters, mode MUXs, and so on), multimode active devices like switches, and MDM circuits and subsystems. Till now, the highest number of on-chip MDM channels is realized by SWG-based ADC, supporting 12 TE modes multiplexed in one single multimode waveguide. The challenge for further higher-order mode multiplexing will be how to relax the fabrication tolerance of coupling efficiency as mode order increases. However, other multimode passive devices, like multimode interfaces, bends, and crossings, still have difficulty supporting more than six modes with high performances. These devices with higher-order mode operation, lower insertion loss, more compact footprint, and even more universal for design are the crucial trends for the future research. Besides, MDM switching networks with optimized routing architecture and compactness for more mode channels are the key challenges to realize large-scale MDM on-chip interconnection. For currently achievable MDM supporting 2–6 modes, hybrid multiplexing with WDM is a reliable method to enhance the total capacity of photonic integrated interconnection and also a long-term trend for on-chip multiplexing. Furthermore, in order to make the bridge between on-chip multimode signals and modes propagating in FMFs, multimode interfaces with low coupling loss and higher reliability are still a big challenge for practical implementation. One cannot use too many modes in a single waveguide for high-density MDM. There are several reasons. One reason is the increased waveguide size, which limits the dense integration and increased fabrication complexity, and bending loss will also be induced. Another reason is the nonlinear distortion due to TPA and Kerr nonlinearity. Si has a high index with a high nonlinear coefficient, which makes Kerr nonlinearity a big issue. At 850 nm, or even O band and C band, TPA is still a problem, which leads to increased loss and noise. One more consideration is the optical interface between MDM PIC and FMF, which typically supports very few modes, like two-mode MDM.

For MDM optical fiber transmission, we review the progresses of FMFs, mode MUXs based on fiber structure, fiber amplifiers for FM systems, and MDM fiber transmission links. We introduced the novel inverse design method for weakly coupled FMFs with high accuracy, high efficiency, and low complexity for fast and reusable fiber designs. Fiber-based mode MUXs, like MSC, LPFBG, and photonic lanterns, provide high efficiency for mode multiplexing, while the fabrication process may be difficult for massive production. FM amplifiers play an essential role for long-haul MDM transmission. DRAs show the advantages of maintaining the MDG for each mode, providing more flexible and customizable designs for FM amplification. Finally, MDM transmission with larger capacity and longer distance is the main target all the time. Key fiber devices reviewed above eventually promote the transmission performances of the whole MDM system. MDM combined with multi-core fibers and WDM shows powerful prospects for next-generation fiber communication with ultra-high capacity.

The implementation requirements need to be considered for MDM in order to make it practical for field applications. As for photonic integration, the on-chip process is rather stable, and MDM devices are quite reliable based on the standard fabrication. The key problem would be the limitation of the optical interface between the PIC and optical fiber, where significant mismatch can be expected between TE/TM modes in the photonic waveguide and LP modes in the fiber. As for optical transmission, MDM can be applied in two scenarios, including brand-new transmission systems with everything compatible with MDM and subsystems like EDFA with SMF input and output but with highly efficient MDM amplification inside. Due to the stability issue, MDM for optical transmission would be challenging, and short reach applications with weak coupling fibers for MIMO-less interconnection are currently more practical.

Generally, one can expect practical applications of MDM for transceivers and active optical cables based on PIC and weak coupling FMFs and amplifier subsystems based on FM-EDFs.

To conclude, MDM technology shows a dominant position to overcome the capacity crunch of optical communications, no matter for chip-scale or short-reach interconnection or long-haul transmission. There are still some challenges for MDM devices and systems (for integrated photonics or fiber optics) to achieve more reliable properties. The core problem includes but is not limited to the methodologies to increase the mode channels and reduce the system cost per channel, improving the compatibility between single-mode and MDM systems at the same time. Further heroic researches and achievements are expectant to be made in the future to lead this area for maintaining the "Moore's law" trend of optical communication.

Acknowledgement

This work was supported by the National Key R&D Program of China (No. 2018YFB1801804) and the National Natural Science Foundation of China (NSFC) (Nos. 61935011, 61875124, and 61675128).

References

1. S. Berdagué and P. Facq, "Mode division multiplexing in optical fibers," Appl. Opt. **21**, 1950 (1982).
2. C. Sun, M. Wade, Y. Lee, J. S. Orcutt, L. Alloatti, M. S. Georgas, A. S. Waterman, J. M. Shainline, R. R. Avizienis, S. Lin, B. R. Moss, R. Kumar, F. Pavanello, A. H. Atabaki, H. M. Cook, A. J. Ou, J. C. Leu, Y.-H. Chen, K. Asanović, R. J. Ram, M. A. Popović, and V. M. Stojanović, "Single-chip microprocessor that communicates directly using light," Nature **528**, 534 (2015).
3. S. C. Gupta, *Textbook on Optical fiber Communication and Its Applications* (PHI Learning Pvt. Ltd., 2018).
4. P. J. Winzer, "Scaling optical fiber networks: challenges and solutions," Opt. Photon. News **26**, 28 (2015).
5. D. Richardson, J. Fini, and L. Nelson, "Space-division multiplexing in optical fibres," Nat. Photon. **7**, 354 (2013).
6. T. Mizuno, H. Takara, K. Shibahara, A. Sano, and Y. Miyamoto, "Dense space division multiplexed transmission over multicore and multimode fiber for long-haul transport systems," J. Lightwave Technol. **34**, 1484 (2016).
7. F. Hamaoka, K. Minoguchi, T. Sasai, A. Matushita, M. Nakamura, S. Okamoto, E. Yamazaki, and Y. Kisaka, "150.3-Tb/s ultra-wideband (S, C, and L bands) single-mode fibre transmission over 40-km using >519 Gb/s/A PDM-128QAM signals," in *European Conference on Optical Communication (ECOC)* (2018).
8. G. Rademacher, B. J. Puttnam, R. S. Luís, J. Sakaguchi, W. Klaus, T. A. Eriksson, Y. Awaji, T. Hayashi, T. Nagashima, T. Nakanishi, T. Taru, T. Takahata, T. Kobayashi, H. Furukawa, and N. Wada, "10.66 peta-bit/s transmission over a 38-core-three-mode fiber," in *Optical Fiber Communication Conference (OFC)* (2020).
9. T. Uematsu, Y. Ishizaka, Y. Kawaguchi, K. Saitoh, and M. Koshiba, "Design of a compact two-mode multi/demultiplexer consisting of multimode interference waveguides and a wavelength-insensitive phase shifter for mode-division multiplexing transmission," J. Lightwave Technol. **30**, 2421 (2012).
10. J. Driscoll, R. Grote, B. Souhan, J. Dadap, M. Lu, and R. Osgood, "Asymmetric Y junctions in silicon waveguides for on-chip mode-division multiplexing," Opt. Lett. **38**, 1854 (2013).
11. W. Chen, P. Wang, and J. Yang, "Mode multi/demultiplexer based on cascaded asymmetric Y-junctions," Opt. Express **21**, 25113 (2013).
12. J. Xing, Z. Li, X. Xiao, J. Yu, and Y. Yu, "Two-mode multiplexer and demultiplexer based on adiabatic couplers," Opt. Lett. **38**, 3468 (2013).
13. C. Sun, Y. Yu, G. Chen, and X. Zhang, "Silicon mode multiplexer processing dual-path mode-division multiplexing signals," Opt. Lett. **41**, 5511 (2016).
14. M. Greenberg and M. Orenstein, "Multimode add-drop multiplexing by adiabatic linearly tapered coupling," Opt. Express **13**, 9381 (2005).
15. D. Dai, C. Li, S. Wang, H. Wu, Y. Shi, Z. Wu, S. Gao, T. Dai, H. Yu, and H. Tsang, "10-channel mode (de)multiplexer with dual polarizations," Laser Photon. Rev. **12**, 1700109 (2018).
16. L. W. Luo, N. Ophir, C. Chen, L. Gabrielli, C. Poitras, K. Bergmen, and M. Lipson, "WDM-compatible mode-division multiplexing on a silicon chip," Nat. Commun. **5**, 3069 (2014).
17. J. Wang, S. Chen, and D. Dai, "Silicon hybrid demultiplexer with 64 channels for wavelength/mode-division multiplexed on-chip optical interconnects," Opt. Lett. **39**, 6993 (2014).
18. R. Baets, A. Z. Subramanian, S. Clemmen, B. Kuyken, P. Bienstman, N. Le Thomas, G. Roelkens, D. Van Thourhout, P. Helin, and S. Severi, "Silicon photonics: silicon nitride versus silicon-on-insulator," in *Optical Fiber Communication Conference* (2016).
19. Y. Yang, Y. Li, Y. Huang, and A. Poon, "Silicon nitride three-mode division multiplexing and wavelength-division multiplexing using asymmetrical directional couplers and microring resonators," Opt. Express **22**, 22172 (2014).
20. J. Hu, V. Tarasov, A. Agarwal, L. Kimerling, N. Carlie, L. Petit, and K. Richardson, "Fabrication and testing of planar chalcogenide waveguide integrated microfluidic sensor," Opt. Express **15**, 2307 (2007).
21. W. C. Tan, M. E. Solmaz, J. Gardner, R. Atkins, and C. Madsen, "Optical characterization of a-As_2S_3 thin films prepared by magnetron sputtering," J. Appl. Phys. **107**, 033524 (2010).
22. C. C. Huang, D. W. Hewak, and J. V. Badding, "Deposition and characterization of germanium sulphide glass planar waveguides," Opt. Express **12**, 2501 (2004).
23. K. E. Youden, T. Grevatt, R. W. Eason, H. N. Rutt, R. S. Deol, and G. Wylangowski, "Pulsed laser deposition of Ga-La-S chalcogenide glass thin film optical waveguides," Appl. Phys. Lett. **63**, 1601 (1993).
24. B. Eggleton, B. L. Davies, and K. Richardson, "Chalcogenide photonics," Nat. Photon. **5**, 141 (2011).
25. W. Shen, P. Zeng, Z. Yang, D. Xia, J. Du, B. Zhang, K. Xu, Z. He, and Z. Li, "Chalcogenide glass photonic integration for improved 2 μm optical interconnection," Photon. Res. **8**, 1484 (2020).
26. R. V. Schmidt and I. P. Kaminow, "Metal-diffused optical waveguides in $LiNbO_3$," Appl. Phys. Lett. **25**, 458 (1974).
27. C. Wang, M. J. Burek, Z. Lin, H. A. Atikian, V. Venkataraman, I.-C. Huang, P. Stark, and M. Lončar, "Integrated high quality factor lithium niobate microdisk resonators," Opt. Express **22**, 30924 (2014).
28. I. Krasnokutska, J. Tambasco, X. Li, and A. Peruzzo, "Ultra-low loss photonic circuits in lithium niobate on insulator," Opt. Express **26**, 897 (2018).
29. R. Wu, M. Wang, J. Xu, J. Qi, W. Chu, Z. Fang, J. Zhang, J. Zhou, L. Qiao, Z. Chai, J. Lin, and Y. Cheng, "Long low-loss-lithium niobate on insulator waveguides with sub-nanometer surface roughness," Nano Mater. **8**, 910 (2018).
30. W. Jin and K. Chiang, "Mode switch based on electro-optic long-period waveguide grating in lithium niobate," Opt. Lett. **40**, 237 (2015).
31. J. Tol, J. Pello, S. Bhat, Y. Jiao, D. Heiss, G. Roelkens, H. Ambrosius, and M. Smit, "Photonic integration in indium-phosphide membranes on silicon (IMOS)," Proc. SPIE **8988**, 89880M (2014).
32. Y. Jiao, J. Pello, A. Mejia, L. Shen, B. Smalbrugge, E. Geluk, M. Smit, and J. Tol, "Fullerene-assisted electron-beam lithography for pattern improvement and loss reduction in InP membrane waveguide devices," Opt. Lett. **39**, 1645 (2014).
33. T. Tanemura, T. Amemiya, K. Takeda, A. Higo, and Y. Nakano, "Simple and compact INP polarization converter for polarization-multiplexed photonic integrated circuits," in *IEEE LEOS Annual Meeting Conference* (2009).
34. F. Guo, D. Lu, R. Zhang, H. Wang, and C. Ji, "A two-mode (de)multiplexer based on multimode interferometer coupler and Y-junction on InP substrate," IEEE Photon. J. **8**, 2700608 (2016).
35. A. M. J. Koonen, H. Chen, H. P. A. van den Boom, and O. Raz, "Silicon photonic integrated mode multiplexer and demultiplexer," IEEE Photon. Technol. Lett. **24**, 1961 (2012).
36. Y. Tong, W. Zhou, X. Wu, and H. K. Tsang, "Efficient mode multiplexer for few-mode fibers using integrated silicon-on-insulator waveguide grating coupler," EEE J. Quantum Electron. **56**, 8400107 (2020).

37. W. Shen, J. Du, J. Xiong, L. Ma, and Z. He, "Silicon-integrated dual-mode fiber-to-chip edge coupler for 2 × 100 Gbps/lambda MDM optical interconnection," Opt. Express **28**, 33254 (2020).
38. Y. Lai, Y. Yu, S. Fu, J. Xu, P. P. Shum, and X. Zhang, "Compact double-part grating coupler for higher-order mode coupling," Opt. Lett. **43**, 3172 (2018).
39. I. Demirtzioglou, C. Lacava, A. Shakoor, A. Khokhar, Y. Jung, D. J. Thomson, and P. Petropoulos, "Apodized silicon photonic grating couplers for mode-order conversion," Photon. Res. **7**, 1036 (2019).
40. M. Zhang, H. Liu, B. Wang, G. Li, and L. Zhang, "Efficient grating couplers for space division multiplexing applications," IEEE J. Sel. Top. Quantum Electron. **24**, 8200605 (2018).
41. H. Chen, V. Sleiffer, B. Snyder, M. Kuschnerov, R. van Uden, Y. Jung, C. Okonkwo, O. Raz, P. O'Brien, H. de Waardt, and T. Koonen, "Demonstration of a photonic integrated mode coupler with 3.072 Tb/s MDM and WDM transmission over few-mode fiber," in *18th OptoElectronics and Communications Conference & 2013 International Conference on Photonics in Switching* (2013).
42. Y. Ding and K. Yvind, "Efficient silicon PIC mode multiplexer using grating coupler array with aluminum mirror for few-mode fiber," in *Conference on Lasers and Electro-Optics (CLEO)* (2015).
43. J. M. Baumann, E. Porto da Silva, Y. Ding, K. Dalgaard, L. H. Frandsen, L. K. Oxenløwe, and T. Morioka, "Silicon chip-to-chip mode-division multiplexing," in *Optical Fiber Communications Conference and Exposition (OFC)* (2018).
44. R. Ryf, N. K. Fontaine, and R. Essiambre, "Spot-based mode couplers for mode-multiplexed transmission in few-mode fiber," IEEE Photon. Technol. Lett. **24**, 1973 (2012).
45. Y. Lai, Y. Yu, S. Fu, J. Xu, P. P. Shum, and X. Zhang, "Efficient spot size converter for higher-order mode fiber-chip coupling," Opt. Lett. **42**, 3702 (2017).
46. Z. Li, Y. Lai, Y. Yu, and X. Zhang, "Reconfigurable fiber-chip mode converter with efficient multi-mode coupling function," IEEE Photon. Technol. Lett. **32**, 371 (2020).
47. D. Dai and M. Mao, "Mode converter based on an inverse taper for multimode silicon nanophotonic integrated circuits," Opt. Express **23**, 28376 (2015).
48. Y. Wu and K. S. Chiang, "Ultra-broadband mode multiplexers based on three-dimensional asymmetric waveguide branches," Opt. Lett. **42**, 407 (2017).
49. X. Jiang, H. Wu, and D. Dai, "Low-loss and low-crosstalk multimode waveguide bend on silicon," Opt. Express **26**, 17680 (2018).
50. Y. Wang and D. Dai, "Ultra-sharp multimode waveguide bends with dual polarizations," J. Lightwave Technol. **38**, 3994 (2020).
51. H. Xie, Y. Liu, W. Li, J. Du, Y. Yao, Q. Song, and K. Xu, "Demonstration of an ultra-compact bend for four modes based on pixelated meta-structure," in *Optical Fiber Communication Conference (OFC)* (2020).
52. X. Wu, W. Zhou, D. Huang, Z. Zhang, Y. Wang, J. Bowers, and H. K. Tsang, "Low crosstalk bent multimode waveguide for on-chip mode-division multiplexing interconnects," in *Conference on Lasers and Electro-Optics* (2018).
53. H. Xu and Y. Shi, "Ultra-sharp multi-mode waveguide bending assisted with metamaterial-based mode converters," Laser Photon. Rev. **12**, 1700240 (2018).
54. C. Sun, Y. Yu, G. Chen, and X. Zhang, "Ultra-compact bent multimode silicon waveguide with ultralow inter-mode crosstalk," Opt. Lett. **42**, 3004 (2017).
55. H. Xie, Y. Liu, Z. Chu, K. Xu, J. Du, and Q. Song, "Ultra-compact dual-mode waveguide bend based on an inverse design," in *The International Photonics and Optoelectronics Meeting (POEM)* (2018).
56. C. Sun, Y. Ding, Z. Li, W. Qi, Y. Yu, and X. Zhang, "Key multimode silicon photonic devices inspired by geometrical optics," ACS Photon. **7**, 2037 (2020).
57. H. Xu and Y. Shi, "Dual-mode waveguide crossing utilizing taper-assisted multimode-interference couplers," Opt. Lett. **41**, 5381 (2016).
58. B. Wu, Y. Yu, and X. Zhang, "Multimode waveguide crossing with ultralow loss and low imbalance," Opt. Express **28**, 14705 (2020).
59. C. Sun, Y. Yu, and X. Zhang, "Ultra-compact waveguide crossing for a mode-division multiplexing optical network," Opt. Lett. **42**, 4913 (2017).
60. W. Chang, L. Lu, X. Ren, L. Lu, M. Cheng, D. Liu, and M. Zhang, "An ultra-compact multimode waveguide crossing based on subwavelength asymmetric Y-junction," IEEE Photon. J. **10**, 4501008 (2018).
61. W. Chang, L. Lu, X. Ren, D. Li, Z. Pan, M. Cheng, D. Liu, and M. Zhang, "Ultracompact dual-mode waveguide crossing based on subwavelength multimode-interference couplers," Photon. Res. **6**, 660 (2018).
62. H. Xu and Y. Shi, "Metamaterial-based Maxwell's fisheye lens for multimode waveguide crossing," Laser Photon. Rev. **12**, 1800094 (2018).
63. H. Xu and Y. Shi, "Ultra-broadband dual-mode 3 dB power splitter based on a Y-junction assisted with mode converters," Opt. Lett. **41**, 5047 (2016).
64. Y. Luo, Y. Yu, M. Ye, C. Sun, and X. Zhang, "Integrated dual-mode 3 dB power coupler based on tapered directional coupler," Sci. Rep. **6**, 23516 (2016).
65. L. Han, B. P.-P. Kuo, N. Alic, and S. Radic, "Ultra-broadband multimode 3 dB optical power splitter using an adiabatic coupler and a Y-branch," Opt. Express **26**, 14800 (2018).
66. W. Chang, X. Ren, Y. Ao, L. Lu, M. Cheng, L. Deng, D. Liu, and M. Zhang, "Inverse design and demonstration of an ultracompact broadband dual-mode 3 dB power splitter," Opt. Express **26**, 24135 (2018).
67. H. Xie, Y. Liu, Y. Wang, Y. Wang, Y. Yao, Q. Song, J. Du, Z. He, and K. Xu, "An ultra-compact 3-dB power splitter for three modes based on pixelated meta-structure," IEEE Photon. Technol. Lett. **32**, 341 (2020).
68. Y. Li, C. Li, C. Li, B. Cheng, and C. Xue, "Compact two-mode (de)multiplexer based on symmetric Y-junction and multimode interference waveguides," Opt. Express **22**, 5781 (2014).
69. Z. Wang, C. Yao, Y. Zhang, and Y. Su, "Ultra-compact and broadband silicon two-mode multiplexer based on asymmetric shallow etching on a multimode interferometer," in *Optical Fiber Communications Conference and Exhibition (OFC)* (2020).
70. Y. Ding, J. Xu, F. Da Ros, B. Huang, H. Ou, and C. Peucheret, "On-chip two-mode division multiplexing using tapered directional coupler-based mode multiplexer and demultiplexer," Opt. Express **21**, 10376 (2013).
71. U. D. Dave and M. Lipson, "Efficient conversion to very high order modes in silicon waveguides," in *Conference on Lasers and Electro-Optics* (2019).
72. Y. Sun, Y. Xiong, and W. N. Ye, "Experimental demonstration of a two-mode (de)multiplexer based on a taper-etched directional coupler," Opt. Lett. **41**, 3743 (2016).
73. J. B. Driscoll, R. R. Grote, B. Souhan, J. I. Dadap, M. Lu, and R. M. Osgood, "Asymmetric Y junctions in silicon waveguides for on-chip mode-division multiplexing," Opt. Lett. **38**, 1854 (2013).
74. W. Chen, P. Wang, T. Yang, G. Wang, T. Dai, Y. Zhang, L. Zhou, X. Jiang, and J. Yang, "Silicon three-mode (de)multiplexer based on cascaded asymmetric Y junctions," Opt. Lett. **41**, 2851 (2016).
75. C. Sun, Y. Yu, M. Ye, G. Chen, and X. Zhang, "An ultra-low crosstalk and broadband two-mode (de)multiplexer based on adiabatic couplers," Sci. Rep. **6**, 38494 (2016).
76. Z. Zhang, Y. Yu, and S. Fu, "Broadband on-chip mode-division multiplexer based on adiabatic couplers and symmetric Y-junction," IEEE Photon. J. **9**, 6600406 (2017).
77. L.-W. Luo, N. Ophir, C. P. Chen, L. H. Gabrielli, C. B. Poitras, K. Bergmen, and M. Lipson, "WDM-compatible mode-division multiplexing on a silicon chip," Nat. Commun. **5**, 3069 (2014).
78. M. Ye, Y. Yu, G. Chen, Y. Luo, and X. Zhang, "On-chip WDM mode-division multiplexing interconnection with optional demodulation function," Opt. Express **23**, 32130 (2015).
79. H. Jia, X. Fu, T. Zhou, L. Zhang, S. Yang, and L. Yang, "Mode-selective modulation by silicon microring resonators and mode multiplexers for on-chip optical interconnect," Opt. Express **27**, 2915 (2019).
80. H. Xiao, Z. Zhang, J. Yang, X. Han, W. Chen, G. Ren, A. Mitchell, J. Yang, D. Gao, and Y. Tian, "On-chip scalable mode-selective converter based on asymmetrical micro-racetrack resonators," Nanophotonics **9**, 1447 (2020).
81. H. Qiu, H. Yu, T. Hu, G. Jiang, H. Shao, P. Yu, J. Yang, and X. Jiang, "Silicon mode multi/demultiplexer based on multimode grating-assisted couplers," Opt. Express **21**, 17904 (2013).
82. C. Gui, Y. Gao, Z. Zhang, and J. Wang, "On-chip silicon two-mode (de)multiplexer for OFDM/OQAM data transmission based on grating-assisted coupler," IEEE Photon. J. **7**, 7905807 (2015).
83. Y. He, Y. Zhang, H. Wang, L. Sun, and Y. Su, "Design and experimental demonstration of a silicon multi-dimensional (de)multiplexer for wavelength-, mode- and polarization-division (de)multiplexing," Opt. Lett. **45**, 2846 (2020).

84. L. F. Frellsen, Y. Ding, O. Sigmund, and L. H. Frandsen, "Topology optimized mode multiplexing in silicon-on-insulator photonic wire waveguides," Opt. Express **24**, 16866 (2016).
85. W. Chang, L. Lu, X. Ren, D. Li, Z. Pan, M. Cheng, D. Liu, and M. Zhang, "Ultra-compact mode (de)multiplexer based on subwavelength asymmetric Y-junction," Opt. Express **26**, 8162 (2018).
86. H. Xie, Y. Liu, S. Wang, Y. Wang, Y. Yao, Q. song, J. Du, Z. He, and K. Xu, "Highly compact and efficient four-mode multiplexer based on pixelated waveguides," IEEE Photon. Technol. Lett. **32**, 166 (2020).
87. H. Xiao, Z. Liu, X. Han, J. Yang, G. Ren, A. Mitchell, and Y. Tian, "On-chip reconfigurable and scalable optical mode multiplexer/demultiplexer based on three-waveguide-coupling structure," Opt. Express **26**, 22366 (2018).
88. W. Jiang, F. Cheng, J. Xu, and H. Wan, "Compact and low-crosstalk mode (de)multiplexer using a triple plasmonic-dielectric waveguide-based directional coupler," J. Opt. Soc. Am. B **35**, 2532 (2018).
89. W. Jiang, "Nonvolatile and ultra-low-loss reconfigurable mode (de)multiplexer/switch using triple-waveguide coupler with $Ge_2Sb_2Se_4Te_1$ phase change material," Sci. Rep. **8**, 15946 (2018).
90. N. Riesen and J. D. Love, "Design of mode-sorting asymmetric Y-junctions," Appl. Opt. **51**, 2778 (2012).
91. Y. Liu, K. Xu, S. Wang, W. Shen, H. Xie, Y. Wang, S. Xiao, Y. Yao, J. Du, Z. He, and Q. Song, "Arbitrarily routed mode-division multiplexed photonic circuits for dense integration," Nat. Commun. **10**, 3263 (2019).
92. D. Chen, X. Xiao, L. Wang, Y. Yu, W. Liu, and Q. Yang, "Low-loss and fabrication tolerant silicon mode-order converters based on novel compact tapers," Opt. Express **23**, 11152 (2015).
93. Y. Zhao, X. Guo, K. Wang, H. Wang, and Y. Su, "Ultra-compact silicon TE-polarized mode converters combining a directional coupler and a phase shifter," in *Asia Communications and Photonics Conference (ACPC)* (2019).
94. J. Xiang, Z. Tao, X. Guo, Y. Zhang, Y. Zhao, and Y. Su, "Universal programmable on-chip metasurface building blocks for arbitrary high-order mode manipulation," arXiv: 2006.08552 (2020).
95. T. Wang, H. Guo, H. Chen, J. Yang, and H. Jia, "Ultra-compact reflective mode converter based on a silicon subwavelength structure," Appl. Opt. **59**, 2754 (2020).
96. H. Jia, H. Chen, T. Wang, H. Xiao, G. Ren, A. Mitchell, J. Yang, and Y. Tian, "Multi-channel parallel silicon mode-order converter for multimode on-chip optical switching," IEEE J. Sel. Top. Quantum Electron. **26**, 8302106 (2020).
97. H. Jia, T. Zhou, X. Fu, J. Ding, and L. Yang, "Inverse-design and demonstration of ultracompact silicon meta-structure mode exchange device," ACS Photon. **5**, 1833 (2018).
98. X. Han, H. Xiao, Z. Liu, T. Zhao, H. Jia, J. Yang, B. J. Eggleton, and Y. Tian, "Reconfigurable on-chip mode exchange for mode-division multiplexing optical networks," J. Lightwave Technol. **37**, 1008 (2019).
99. J. Guo, C. Ye, C. Liu, M. Zhang, C. Li, J. Li, and D. Dai, "Ultra-compact and ultra-broadband guided-mode exchangers on silicon," Laser Photon. Rev. **14**, 2000058 (2020).
100. X. Guan, Y. Ding, and L. H. Frandsen, "Ultra-compact broadband higher order-mode pass filter fabricated in a silicon waveguide for multimode photonics," Opt. Lett. **40**, 3893 (2015).
101. C. Sun, W. Wu, Y. Yu, X. Zhang, and G. T. Reed, "Integrated tunable mode filter for a mode-division multiplexing system," Opt. Lett. **43**, 3658 (2018).
102. D. Dai, "Silicon polarization beam splitter based on an asymmetrical evanescent coupling system with three optical waveguides," J. Lightwave Technol. **30**, 3281 (2012).
103. H. Qiu, J. Jiang, P. Yu, J. Yang, H. Yu, and X. Jiang, "Broad bandwidth and large fabrication tolerance polarization beam splitter based on multimode anti-symmetric Bragg sidewall gratings," Opt. Lett. **42**, 3912 (2017).
104. H. Qiu, J. Jiang, P. Yu, T. Dai, J. Yang, H. Yu, and X. Jiang, "Silicon band-rejection and band-pass filter based on asymmetric Bragg sidewall gratings in a multimode waveguide," Opt. Lett. **41**, 2450 (2016).
105. J. Jiang, H. Qiu, G. Wang, Y. Li, T. Dai, D. Mu, H. Yu, J. Yang, and X. Jiang, "Silicon lateral-apodized add–drop filter for on-chip optical interconnection," Appl. Opt. **56**, 8425 (2017).
106. H. Qiu, J. Jiang, T. Hu, P. Yu, J. Yang, X. Jiang, and H. Yu, "Silicon add-drop filter based on multimode Bragg sidewall gratings and adiabatic couplers," J. Lightwave Technol. **35**, 1705 (2017).
107. J. Jiang, H. Qiu, G. Wang, Y. Li, T. Dai, X. Wang, H. Yu, J. Yang, and X. Jiang, "Broadband tunable filter based on the loop of multimode Bragg grating," Opt. Express **26**, 559 (2018).
108. H. Xu and Y. Shi, "Ultra-compact and highly efficient polarization rotator utilizing multi-mode waveguides," Opt. Lett. **42**, 771 (2017).
109. H. Xu and Y. Shi, "Ultra-broadband silicon polarization splitter-rotator based on the multi-mode waveguide," Opt. Express **25**, 18485 (2017).
110. C. Sun, Y. Yu, Y. Ding, Z. Li, W. Qi, and X. Zhang, "Integrated mode-transparent polarization beam splitter supporting thirteen data channels," Photon. Res. **8**, 978 (2020).
111. G. Zhou, L. Zhou, Y. Guo, S. Chen, Z. Fu, L. Lu, and J. Chen, "High-speed silicon electro-optic modulator based on a single multimode waveguide," in *Optical Fiber Communication Conference* (2019).
112. S. Miller, Y. Chang, C. Phare, M. Shin, M. Zadka, S. Roberts, B. Stern, X. Ji, A. Mohanty, O. Jimenez Gordillo, U. Dave, and M. Lipson, "Large-scale optical phased array using a low-power multi-pass silicon photonic platform," Optica **7**, 3 (2020).
113. M. Ye, Y. Yu, C. Sun, and X. Zhang, "On-chip data exchange for mode division multiplexed signals," Opt. Express **24**, 528 (2016).
114. C. Sun, Y. Yu, G. Chen, and X. Zhang, "Integrated switchable mode exchange for reconfigurable mode-multiplexing optical networks," Opt. Lett. **41**, 3257 (2016).
115. C. Sun, Y. Yu, G. Chen, and X. Zhang, "On-chip switch for reconfigurable mode-multiplexing optical network," Opt. Express **24**, 21722 (2016).
116. Y. Xiong, R. B. Priti, and O. Liboiron-Ladouceur, "High-speed two-mode switch for mode-division multiplexing optical networks," Optica **4**, 1098 (2017).
117. H. Jia, S. Yang, T. Zhou, L. Zhang, T. Wang, H. Chen, J. Yang, and L. Yang, "Mode-oriented permutation cipher encryption and passive signal switching based on multiobjective optimized silicon subwavelength metastructures," ACS Photon. **7**, 2163 (2020).
118. L. Lu, D. Liu, M. Yan, and M. Zhang, "Subwavelength adiabatic multimode Y-junctions," Opt. Lett. **44**, 4729 (2019).
119. S. A. Miller, Y.-C. Chang, C. T. Phare, M. C. Shin, M. Zadka, S. P. Roberts, B. Stern, X. Ji, A. Mohanty, O. A. J. Gordillo, U. D. Dave, and M. Lipson, "Large-scale optical phased array using a low-power multi-pass silicon photonic platform," Optica **7**, 3 (2020).
120. D. Dai and J. E. Bowers, "Silicon-based on-chip multiplexing technologies and devices for peta-bit optical interconnects," Nanophotonics **3**, 283 (2014).
121. H. Jia, S. Yang, T. Zhou, S. Shao, X. Fu, L. Zhang, and L. Yang, "WDM-compatible multimode optical switching system-on-chip," Nanophotonics **8**, 889 (2019).
122. B. Stern, X. Zhu, C. P. Chen, L. D. Tzuang, J. Cardenas, K. Bergman, and M. Lipson, "On-chip mode-division multiplexing switch," Optica **2**, 530 (2015).
123. H. Jia, T. Zhou, L. Zhang, J. Ding, X. Fu, and L. Yang, "Optical switch compatible with wavelength division multiplexing and mode division multiplexing for photonic networks-on-chip," Opt. Express **25**, 20698 (2017).
124. Y. Zhang, Q. Zhu, Y. He, C. Qiu, Y. Su, and R. Soref, "Silicon 1 × 2 mode- and polarization-selective switch," in *Optical Fiber Communication Conference* (2017).
125. L. Yang, T. Zhou, H. Jia, S. Yang, J. Ding, X. Fu, and L. Zhang, "General architectures for on-chip optical space and mode switching," Optica **5**, 180 (2018).
126. C. Sun, W. Wu, Y. Yu, G. Chen, X. Zhang, X. Chen, D. J. Thomson, and G. T. Reed, "De-multiplexing free on-chip low-loss multimode switch enabling reconfigurable inter-mode and inter-path routing," Nanophotonics **7**, 1571 (2018).
127. D. Zhou, C. Sun, Y. Lai, Y. Yu, and X. Zhang, "Integrated silicon multifunctional mode-division multiplexing system," Opt. Express **27**, 10798 (2019).
128. S. Wang, H. Wu, H. K. Tsang, and D. Dai, "Monolithically integrated reconfigurable add-drop multiplexer for mode-division-multiplexing systems," Opt. Lett. **41**, 5298 (2016).
129. S. Wang, X. Feng, S. Gao, Y. Shi, T. Dai, H. Yu, H.-K. Tsang, and D. Dai, "On-chip reconfigurable optical add-drop multiplexer for hybrid wavelength/mode-division-multiplexing systems," Opt. Lett. **42**, 2802 (2017).
130. L. Han, B. P. Kuo, N. Alic, and S. Radic, "Silicon photonic wavelength and mode selective switch for WDM-MDM networks," in *Optical Fiber Communications Conference and Exhibition (OFC)* (2019).

131. R. Maruyama, N. Kuwaki, S. Matsuo, and M. Ohashi, "Experimental investigation of relation between mode-coupling and fiber characteristics in few-mode fibers," in *Optical Fiber Communication Conference* (2015).
132. P. Sillard, M. Bigot-Astruc, D. Boivin, H. Maerten, and L. Provost, "Few-mode fiber for uncoupled mode-division multiplexing transmissions," in *37th European Conference and Exposition on Optical Communications* (2011).
133. M. Bigot-Astruc, D. Boivin, and P. Sillard, "Design and fabrication of weakly-coupled few-modes fibers," in *IEEE Photonics Society Summer Topical Meeting Series* (2012).
134. M. Bigot, D. Molin, K. de Jongh, D. Van Ras, F. Achten, and P. Sillard, "Next-generation multimode fibers for space division multiplexing," in *Advanced Photonics* (2017).
135. S. Jiang, L. Ma, Z. Zhang, X. Xu, S. Wang, J. Du, C. Yang, W. Tong, and Z. He, "Design and characterization of ring-assisted few-mode fibers for weakly coupled mode-division multiplexing transmission," J. Lightwave Technol. **36**, 5547 (2018).
136. L. Ma, S. Jiang, J. Du, C. Yang, W. Tong, and Z. He, "Ring-assisted 7-LP-mode fiber with ultra-low inter-mode crosstalk," in *Asia Communications and Photonics Conference* (2016).
137. K. Sato, R. Maruyama, N. Kuwaki, S. Matsuo, and M. Ohashi, "Optimized graded index two-mode optical fiber with low DMD, large A_{eff} and low bending loss," Opt. Express **21**, 16231 (2013).
138. P. Sillard, D. Molin, M. Bigot-Astruc, K. De Jongh, F. Achten, A. M. Velázquez-Benítez, R. Amezcua-Correa, and C. M. Okonkwo, "Low-differential-mode-group-delay 9-LP-mode fiber," J. Lightwave Technol. **34**, 425 (2016).
139. Y. Kim, H. E. Engan, H. J. Shaw, and J. N. Blake, "Fiber-optic modal coupler using periodic microbending," Opt. Lett. **11**, 389 (1986).
140. J. N. Blake, B. Y. Kim, and H. J. Shaw, "Highly selective evanescent modal filter for two-mode optical fibers," Opt. Lett. **11**, 177 (1986).
141. J. Liang, Q. Mo, S. Fu, M. Tang, P. Shum, and D. Liu, "Design and fabrication of elliptical-core few-mode fiber for MIMO-less data transmission," Opt. Lett. **41**, 3058 (2016).
142. L. Wang and S. LaRochelle, "Design of eight-mode polarization-maintaining few-mode fiber for multiple-input multiple-output-free spatial division multiplexing," Opt. Lett. **40**, 5846 (2015).
143. C. Xia, N. Bai, I. Ozdur, X. Zhou, and G. Li, "Supermodes for optical transmission," Opt. Express **19**, 16653 (2011).
144. H. Xiao, H. Li, G. Ren, Y. Dong, S. Xiao, J. Liu, B. Wei, and S. Jian, "Polarization-maintaining supermode fiber supporting 20 modes," IEEE Photon. Technol. Lett. **29**, 1340 (2017).
145. Z. He, J. Du, W. Shen, Y. Huang, C. Wang, K. Xu, and Z. He, "Inverse design of few-mode fiber by neural network for weak-coupling optimization," in *Optical Fiber Communication Conference* (2020).
146. G. Stepniak, L. Maksymiuk, and J. Siuzdak, "Increasing multimode fiber transmission capacity by mode selective spatial light phase modulation," in *36th European Conference and Exhibition on Optical Communication* (2010).
147. L. Zhu, X. Wei, J. Wang, Z. Zhang, Z. Li, H. Zhang, S. Li, K. Wang, and J. Liu, "Experimental demonstration of basic functionalities for 0.1-THz orbital angular momentum (OAM) communications," in *Optical Fiber Communication Conference* (2014).
148. J. Li, "A study on key technologies for mode division multiplexed optical transmission systems," Ph.D. Thesis (Shanghai Jiao Tong University, 2019).
149. K. Y. Song, I. K. Hwang, S. H. Yun, and B. Y. Kim, "High performance fused-type mode-selective coupler using elliptical core two-mode fiber at 1550 nm," IEEE Photon. Technol. Lett. **14**, 501 (2002).
150. S. Savin, M. J. F. Digonnet, G. S. Kino, and H. J. Shaw, "Tunable mechanically induced long-period fiber gratings," Opt. Lett. **25**, 710 (2000).
151. S. G. Leon-Saval, N. K. Fontaine, and R. Amezcua-Correa, "Photonic lantern as mode multiplexer for multimode optical communications," Opt. Fiber Tech. **35**, 46 (2017).
152. N. K. Fontaine, R. Ryf, J. Bland-Hawthorn, and S. G. Leon-Saval, "Geometric requirements for photonic lanterns in space division multiplexing," Opt. Express **20**, 27123 (2012).
153. Y. Jung, S. Alam, Z. Li, A. Dhar, D. Giles, I. P. Giles, J. K. Sahu, F. Poletti, L. Grüner-Nielsen, and D. J. Richardson, "First demonstration and detailed characterization of a multimode amplifier for space division multiplexed transmission systems," Opt. Express **19**, B952 (2011).
154. G. L. Cocq, L. Bigot, A. L. Rouge, M. Bigot-Astruc, P. Sillard, C. Koebele, M. Salsi, and Y. Quiquempois, "Modeling and characterization of a few-mode EDFA supporting four mode groups for mode division multiplexing," Opt. Express **20**, 27051 (2012).
155. Q. Kang, E. Lim, Y. Jung, F. Poletti, S. Alam, and D. J. Richardson, "Design of four-mode erbium doped fiber amplifier with low differential modal gain for modal division multiplexed transmissions," in *Optical Fiber Communication Conference* (2013).
156. Y. Wakayama, K. Igarashi, D. Soma, H. Taga, and T. Tsuritani, "Novel 6-mode fibre amplifier with large erbium-doped area for differential modal gain minimization," in *42nd European Conference on Optical Communication* (2016).
157. A. Gaur, G. Kumar, and V. Rastogi, "Dual-core few mode EDFA for amplification of 20 modes," Opt. Quantum Electron. **50**, 66 (2018).
158. L. Bigot, J. Trinel, G. Bouwmans, E. R. Andresen, and Y. Quiquempois, "Few-mode and multicore fiber amplifiers technology for SDM," in *Optical Fiber Communication Conference* (2018).
159. G. Khanna, T. Rahman, E. D. Man, E. Riccardi, A. Pagano, A. C. Piat, S. Calabrò, B. Spinnler, D. Rafique, and U. Feiste, "Single-carrier 400G 64QAM and 128QAM DWDM field trial transmission over metro legacy links," IEEE Photon. Tech. Lett. **29**, 189 (2017).
160. S. Namiki and Y. Emori, "Ultrabroad-band Raman amplifiers pumped and gain-equalized by wavelength-division-multiplexed high-power laser diodes," IEEE J. Sel. Top. Quantum. Electron. **7**, 3 (2001).
161. R. Ryf, A. Sierra, R.-J. Essiambre, S. Randel, A. H. Gnauck, C. Bolle, M. Esmaeelpour, P. J. Winzer, R. Delbue, P. Pupalaikise, A. Sureka, D. W. Peckham, A. McCurdy, and R. Lingle, "Mode-equalized distributed Raman amplification in 137-km few-mode fiber," *in European Conference and Exhibition on Optical Communication* (2011).
162. M. Esmaeelpour, R. Ryf, N. K. Fontaine, H. Chen, A. H. Gnauck, R. Essiambre, J. Toulouse, Y. Sun, and R. Lingle, "Transmission over 1050-km few-mode fiber based on bidirectional distributed Raman amplification," J. Lightwave Technol. **34**, 1864 (2016).
163. J. Li, L. Wang, J. Du, S. Jiang, L. Ma, C. Cai, L. Zhu, A. Wang, M.-J. Li, H. Chen, J. Wang, and Z. He, "Experimental demonstration of a few-mode Raman amplifier with a flat gain covering 1530–1605 nm," Opt. Lett. **43**, 4530 (2018).
164. J. Li, J. Du, L. Ma, M.-J. Li, K. Xu, and Z. He, "Second-order few-mode Raman amplifier for mode-division multiplexed optical communication systems," Opt. Express **25**, 810 (2017).
165. J. Li, C. Cai, J. Du, S. Jiang, and Z. He, "Ultra-low-noise mode-division multiplexed WDM transmission over 100-km FMF based on a second-order few-mode Raman amplifier," J. Lightwave Technol. **36**, 3254 (2018).
166. J. D. Ania-Castañón, "Quasi-lossless transmission using second-order Raman amplification and fibre Bragg gratings," Opt. Express **12**, 4372 (2004).
167. M. Tan, P. Rosa, S. T. Le, V. V. Dvoyrin, M. A. Iqbal, S. Sugavanam, S. K. Turitsyn, and P. Harper, "RIN mitigation and transmission performance enhancement with forward broad band pump," IEEE Photon. Technol. Lett. **30**, 254 (2018).
168. Y. Chen, J. Du, J. Li, L. Shen, J. Luo, and Z. He, "Time-wavelength-mode equalization by PSO for random fiber laser based FMF Raman amplifier," in *Optical Fiber Communication Conference* (2020).
169. Y. Chen, J. Du, Y. Huang, K. Xu, and Z. He, "Intelligent gain flattening of FMF Raman amplification by machine learning based inverse design," in *Optical Fiber Communication Conference* (2020).
170. Y. Chen, J. Du, Y. Huang, K. Xu, and Z. He, "Intelligent gain flattening in wavelength and space domain for FMF Raman amplification by machine learning based inverse design," Opt. Express **28**, 11911 (2020).
171. S. Berdagué and P. Facq, "Mode division multiplexing in optical fibers," Appl. Opt. **21**, 1950 (1982).
172. E. Ip, N. Bai, Y. K. Huang, E. Mateo, F. Yaman, M. J. Li, S. Bickham, S. Ten, J. Liñares, C. Montero, V. Moreno, X. Prieto, V. Tse, K. M. Chung, A. Lau, H. Y. Tam, C. Lu, Y. Luo, G. D. Peng, and G. Li, "$88 \times 3 \times 112$-Gb/s WDM transmission over 50 km of three-mode fiber with inline few mode fiber amplifier," in *37th European Conference and Exposition on Optical Communications* (2011).
173. R. Ryf, S. Randel, A. H. Gnauck, C. Bolle, A. Sierra, S. Mumtaz, M. Esmaeelpour, E. C. Burrows, R. Essiambre, P. J. Winzer, D. W. Peckham, A. H. McCurdy, and R. Lingle, "Mode-division

multiplexing over 96 km of few-mode fiber using coherent 6 ×6 MIMO processing," J. Lightwave Technol. **30**, 521 (2012).
174. S. Randel, R. Ryf, A. H. Gnauck, M. A. Mestre, C. Schmidt, R.-J. Essiambre, P. J. Winzer, R. Delbue, P. Pupalaikis, A. Sureka, Y. Sun, X. Jiang, and R. Lingle, "Mode-multiplexed 6×20-GBd QPSK transmission over 1200-km DGD-compensated few-mode fiber," in *National Fiber Optic Engineers Conference* (2012).
175. D. Soma, K. Igarashi, Y. Wakayama, K. Takeshima, Y. Kawaguchi, N. Yoshikane, T. Tsuritani, I. Morita, and M. Suzuki, "2.05 peta-bit/s super-Nyquist-WDM SDM transmission using 9.8-km 6-mode 19-core fiber in full C band," in *European Conference on Optical Communication* (2015).
176. R. Ryf, H. Chen, N. K. Fontaine, A. M. Velazquez-Benitez, J. Antonio-Lopez, J. C. Alvarado, Z. Sanjabi Eznaveh, C. Jin, B. Huang, S. H. Chang, B. Ercan, C. Gonnet, M. Bigot-Astruc, D. Molin, F. Achten, P. Sillard, and R. Amezcua-Correa, "10-mode mode-multiplexed transmission with inline amplification," in *42nd European Conference on Optical Communication* (2016).
177. D. Soma, Y. Wakayama, S. Beppu, S. Sumita, T. Tsuritani, T. Hayashi, T. Nagashima, M. Suzuki, H. Takahashi, K. Igarashi, I. Morita, and M. Suzuki, "10.16 peta-bit/s dense SDM/WDM transmission over low-DMD 6-mode 19-core fibre across C+L band," in *European Conference on Optical Communication (ECOC)* (2017).
174. G. Rademacher, R. Ryf, N. K. Fontaine, H. Chen, R. J. Essiambre, B. J. Puttnam, R. S. Luís, Y. Awaji, N. Wada, S. Gross, N. Riesen, M. Withford, Y. Sun, and R. Lingle, "Long-haul transmission over few-mode fibers with space-division multiplexing," J. Lightwave Technol. **36**, 1382 (2018).
179. G. Rademacher, R. S. Luís, B. J. Puttnam, T. A. Eriksson, R. Ryf, E. Agrell, R. Maruyama, K. Aikawa, Y. Awaji, H. Furukawa, and N. Wada, "High-capacity transmission with few-mode fibers," J. Lightwave Technol. **37**, 425 (2019).
180. K. Shibahara, T. Mizuno, D. Lee, Y. Miyamoto, H. Ono, K. Nakajima, Y. Amma, K. Takenaga, and K. Saitoh, "DMD-unmanaged long-haul SDM transmission over 2500-km 12-core × 3-mode MC-FMF and 6300-km 3-mode FMF employing intermodal interference canceling technique," J. Lightwave Technol. **37**, 138 (2019).
181. K. Shibahara, T. Mizuno, H. Ono, K. Nakajima, and Y. Miyamoto, "Long-haul DMD-unmanaged 6-mode-multiplexed transmission employing cyclic mode-group permutation," in *Optical Fiber Communication Conference* (2020).